공학박사 학위논문

Capillarity Guided Patterning of Microliquids

모세관 현상을 이용한 미소 액체 패터닝 기법

2015년 8월

서울대학교 대학원

기계항공공학부

강 명 우

Abstract

Capillarity Guided Patterning of Microliquids

Myeongwoo Kang
Department of Mechanical and Aerospace Engineering
The Graduate School
Seoul National University

Soft lithography and other techniques have been developed to investigate biological and chemical phenomena as an alternative to photolithography-based patterning methods that have compatibility problems. This paper describes a simple and novel approach for non-lithographic patterning of liquids and gels. Using a design that incorporates strategically placed microstructures, micro-liquids or gels can be spontaneously trapped and patterned using the surface tension between liquid and microstructures. The main advantage of this method is simplicity. Various liquid patterns with ~1nL were patterned by simple liquid draining or wiping motion. This method is geometrically analyzed based on hydrodynamics and verified with simulation and experiments. Various materials (i.e. water, hydrogels

and other liquids) have been successfully patterned with complex shapes that are isolated from each other. Multiple cell types are patterned within the gels. Capillarity guided patterning is fast, simple and robust. It is not limited by pattern shape, size, cell type and material. The simplicity and robustness of the capillarity guided patterning will be attractive in developing novel in-vitro models of organ-on-a-chip, high-throughput screening and other biological experimental platforms amenable to long-term observation of dynamic events using advanced imaging and analytical techniques.

Keywords: Lab-on-a-chip, Liquid patterning, Microfluidics, Surface tension, High-throughput screening, Organ-on-a-chip

Student Number: 2012-30732

Contents

List of Figures

Chapter 1.

Introduction

Despite the short history, non-conventional microscale patterning techniques such as soft lithography have matured considerably in recent years. [1-5] Micropatterning techniques offer many advantages over conventional large scale methods based on photolithography and in biological research. Conventional research tools have severe limitations in terms of compatibility in handling live cells. Alternatives such soft lithography and others have been developed to fill this gap of single cell patterening/manipulation [6-11], production of complex chemical gradients [12], patterning for co-culture tissue engineering [13-17] and others. Non-conventional, “soft” micropatterning techniques have gained considerable appeal for biological and chemical research. [14, 16, 18-21]

One of the widely adopted method for cell patterning is based on soft lithography techniques such as microcontact printing (μCP) [22] and micro-molding in capillaries (MIMIC) [1, 18]. Microcontact printing and MIMIC transfer protein or extracellular matrix (ECM) patterns on a substrate which is used for selective cell attachment. [23] Although these methods can make small and precise patterns, they can be only applied to the adherent cells and require additional processes such as metal deposition and etching or oxidation. [24] Furthermore, μCP and MIMIC can produce limited patterns such as lines or spots and it is difficult to produce functional multicellular patterns or co-cultures with 3 or more cell types. [25]

Recently, many efforts have been devoted to pattern cells on 2D surfaces or in 3D gels to mimic *in-vivo* microenvironment. Cells were patterned within hydrogels (i.e. collagen or others) [26, 27], UV curable materials (i.e. PEG-DA) [14, 28, 29] and droplets [30, 31].

Another approach to fix the cell position is using external forces to move cells to specific positions by optical tweezers, digitalized Braille pins [32, 33], micro-traps using hydrodynamics [19, 34-37] and dielectrophoresis. [12] These techniques provide more advanced patterning capability and cell compatibility.

In this study, we introduce new methods for rapid patterning in two ways; by simple aspiration and by simple wiping. Based on understanding of the hydrodynamics, we have designed structures to control the shape of menisci and their dynamics to generate complex micro-liquid patterns of variable size and shapes. Using this new technique called capillarity-guided patterning (CGP), we demonstrated variety of patterns of cells trapped in hydrogel and cancer-HUVEC co-culture). Furthermore, we could produce complex patterns consisting of multiple materials (or materials with different composition). Compared to other patterning methods,

capillarity guided patterning is: (i) extremely simple and fast, (ii) robust and reliable, (iii) flexible in terms of possible pattern shape, size and material, (iv) no need for special equipment or complex processes, and (v) scalable to large area patterning.

We expect capillarity guided patterning to become a new method of microscale patterning based on fluid mechanics principles. Capillarity guided patterning provide simplicity and robustness and it will be attractive in developing novel biological experimental platforms such as organ-on-a-chip and high throughput screening system.

Chapter 2.

Capillarity Guided Patterning of Microliquids

2.1 Introduction

Microfluidics-based research has several advantages compared to conventional laboratory-scale analytical processes because it offers faster and more sensitive detection with a smaller reagent volume. [1, 37-39] Microfluidic technology enables the integration of an entire laboratory on a single chip. [11, 40, 41] For advanced lab-on-a-chip operations, microfluidic devices may require complex 3D structures that can integrate various functions, such as a mixer, a fluidic isolation channel, and valves. Microfluidic approaches are being increasingly used in performing cell-based assays and other applications. [13, 18, 21, 23, 42, 43]

The most important application of microfluidic based bio-chemical research is high throughput screening. [8, 34, 44] High throughput screening is a powerful tool for biomedical engineering such as cell metabolism, cell-to-cell interaction, diagnostics and drug discovery. [45-48]Microfluidic platform has many advantages for high throughput screening like laminar flow, low diffusion, easy cytometry and flow control using microstructures. [49-53]

Another microfluidic application is ‘Organ-on-chips’. This is a technique for investigation of cells and tissues interaction to understand the function and pathophysiology of living organs. The existing conventional *in vitro* methods have limitations to mimic complex specifications such as three dimensional (3D) structures and co-culture. [54-56] However, the microfluidic techniques enable mimicking real organ successfully by using the advantages of microfluidics; fluidic isolation, cell positioning, 3D multicellular

culture, tunable flow and spatiotemporal gradient. [10, 19, 31, 57, 58]

For high throughput screening and organ-on-chips application, fixed region of interest (ROI) is important issue for data analysis and cell positioning. [14, 59-62] There are many methods to fix the ROI using extra cellular matrix (ECM) or chemical patterning, optical tweezer, droplet formation, UV curable polymer lithography, pneumatic valve and hydrodynamics. Current approaches can fix the ROI effectively but those methods require additional processes and equipment. [31, 32, 63-65]

In this study, we introduce new method for rapid liquid patterning on microfluidic platform. This technique is based on the hydrodynamics using surface tension of the liquid. Compared with the existing methods, our new technique can produce any shape of liquid patterns, including multiple liquid patterns, using the geometry of post arrays within 5 seconds and it doesn’t require additional

processes and equipment like surface treatment (chemicals or ECM) or pumping systems.

2.2 Materials and methods

2.2.1 Microfluidic device fabrication

Microfluidic devices were fabricated using soft lithography. Master molds for soft lithography were fabricated by patterning negative tone photoresist SU8-100 (MicroChem, Newton, MA) with 100 μm thickness on Si wafers (Silicon Sense, Boise, ID) by typical photolithography. Positive replicas with embossed channels were fabricated by molding polydimethylsiloxane (PDMS; Sylgard 184, Dow Corning, Midland, MI) against the master mold. The PDMS prepolymer was mixed with curing agent by 10:1(w/w) ratio. The PDMS poured master was placed on hot plate (95℃) for curing PDMS. Cured PDMS was then separated and inlet and outlet reservoirs for fluidic interconnects were punched with sharpened needles. The PDMS piece was irreversibly bonded to a glass slide

upon treating both with an air-plasma generator (Femto Science, South Korea), forming the microfluidic device. (Figure 2.1)

2.2.2 Modeling of meniscus dynamics

A two-dimensional simulation was performed using Matlab (MathWorks, Natick, MA) and COMSOL Multiphysics (Comsol, Palo Alto, CA) to model the dynamics of meniscus at liquid-air interface with.

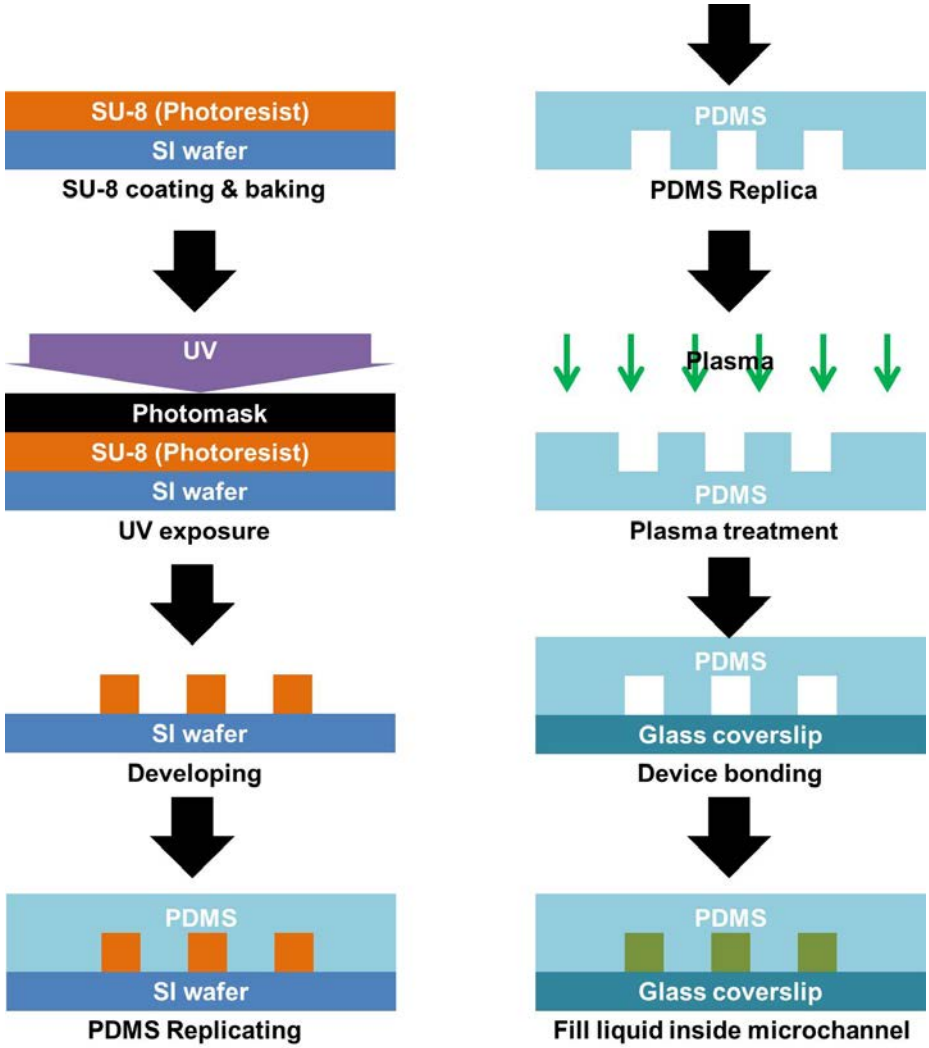

Figure 2. 1 Microfluidic device fabrication process.

2.2.3 Cell Culture

Chlamydomonas reinhardtii (CC-503) in tris acetate phosphate (TAP) medium were cultured at 23 °C and 5% CO2 while shaking on an orbital shaker at 125 rpm. The cultures were exposed to 12 h cycles of light (40 μmol/s m^2) and dark.

Primary cortical neurons were extracted from embryonic Sprague-Dawley rats (TP18). Cortices were extracted and dissected in 1× Hank's balanced salt solution (HBSS). Then it was treated with 3 mL of 0.125% trypsin/ethylenediaminetetraacetic acid (EDTA) for 15 min in a 37°C water bath. The trypsin/EDTA was removed by rinsing three times with HBSS, after which 1 mL of plating medium Dulbecco's Modified Eagle Medium (DMEM) with 10% fetal bovine solution (FBS) was added, and the mixture was centrifuged for 1 min at 1,100 rpm. The supernatant was then discarded, and 2 mL of a

neurobasal medium(Gibco) containing 2% of supplement B-27, 0.25% GlutaMax media supplement, and 1% Pen/Strep (Invitrogen, Carlsbad, CA) was added. The cells were triturated using a Pasteur pipette. The cell suspension was filtered through a cell strainer with a pore size of 22 μm, and the cell viability and density were determined by trypan blue staining. All procedures performed were approved by the Institute of Laboratory Animal Resources (ILAR) at Seoul National University, Korea.

Human umbilical vein endothelial cells (HUVEC, Lonza) were cultured in Endothelial Growth Medium (EGM-2, Lonza). Normal human lung fibroblasts (LF, Lonza) were cultured in Fibroblast Growth Medium (FGM-2, Lonza). Human glioblastoma multiforme cells, U87MG (ATCC, Virginia) were cultured in DMEM supplemented with 10% FBS, penicillin (100 Units/mL) and streptomycin (100 Units/mL). All cells were cultured in a humidified

incubator at 37°C and 5% CO_2.

2.2.4 Cell Loading

Chlamydomonas reinhardtii suspension was mixed in 1:1 ratio with alginate solution (8%, w/v) with final concentration 5×10^6 cells/mL. It was polymerized by introducing $CaCl_2$ (10%, w/v).

Primary rat cortical neurons were mixed with matrigel (BD Science) in 1:1 ratio with final concentration of 6×10^6 cells/mL and polymerized after aspiration. With culture media filled inside the channel, it was incubated for 5 days to form a network (Figure 5B).

To obtained designed blood vessel network as shown in Figure 5C, HUVECs were suspended in fibrinogen solution (2.5 mg/mL fibrinogen with 0.15 Units/mL of aprotinin and 0.5 Units/mL of thrombin) at a concentration of 15×10^6 cells/mL and patterned

using CGP. After aspiration, the cell-fibrin mixture was placed in an incubator for two minutes for polymerization. The microchannel was loaded with EGM-2 medium with LFs at a concentration of 1.5 x 10^6 cells/mL. Devices were incubated for 4~5 days and media was changed every 2 days to obtain lumenized blood vessel.

For in-vitro cancer angiogenesis model as shown in Figure 2.15, U87MGs were mixed with fibrinogen solution at a concentration of 6 x 10^6 cells/mL. Mixture was injected and quickly aspirated to trap the cancer cells inside the circular pattern. After two minutes of incubation to obtain crosslinked fibrin, HUVEC and LF mixture with fibrinogen solution with concentration of 10 x 10^6 cells/mL and 10^6 cells/mL, respectively, were injected into the channel then cured. EGM-2 media was added to the reservoirs at the each end of the channel and remained in the incubator with media change every other day.

2.2.5 PEG-DA photopolymerization

To perform multiple material patterning, UV curable polymer, poly(ethylene glycol) diacrylate (PEG-DA, MW: 258, mixed with 3%DMPA for photo initiator) mixed with color ink was used. PEG-DA was cross-linked with a UV lamp (22 mW/cm^2) for 15 seconds.

2.2.6 Immunostaining

To image *Chlamydomonas reinhardtii*, auto-fluorescence signal from chlorophyll was used. Primary rat cortical neurons were stained with Calcein AM (Molecular Probes). For imaging endothelial cells, mouse monoclonal antibody specific for human CD31 (AlexaFluor1647, clone WM59, BioLegends) were used and Hoechst 33342 (Molecular Probes) was used to stain the nuclei.

CellTracker™ Green CMFDA (5-chloromethylfluorescein diacetate, Molecular Probes) was used to stain U87MG cancer cells. All cells were stained before loading.

2.2.7 Imaging

Olympus FV1000 confocal microscope was used for 3D cross-sectional imaging. Images were analyzed with imageJ and IMARIS (Bitplane, Switzerland).

2.3 Results

2.3.1 Meniscus dynamics with microstructures

We first describe the dynamics of liquid meniscus that advances and snaps as the volume of liquid decreases in the microchannel. Figure 2.2 shows the schematic of the experimental setup for observing meniscus dynamics when liquid filled channel is drained. The device design incorporates a number of posts strategically positioned within the main microchannel. When a liquid-filled microchannel is drained, liquid-air interface contacting the posts form a number of menisci along the channel width. When the meniscus touches the posts, the interface straddling the posts advances first while the contact line on the post surface moves around it. Thus, the meniscus bulges into the liquid region. The shape of meniscus is influenced by the property of liquid-solid interaction (surface tension)

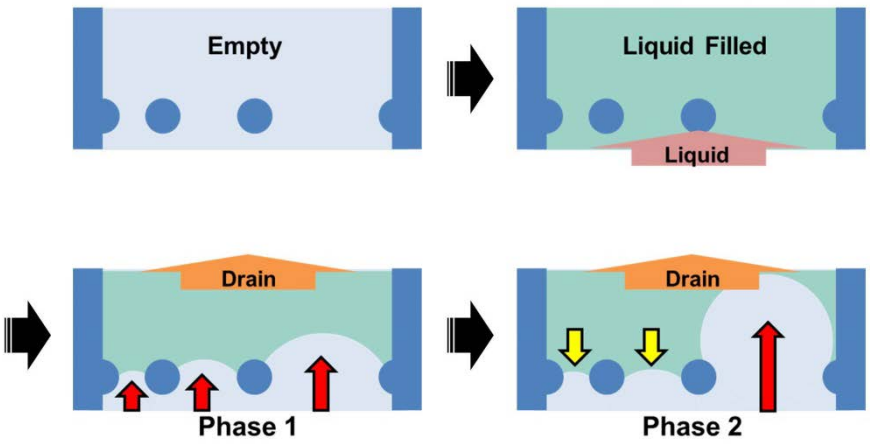

Figure 2. 2 Simplified schematic of microchannel containing isolated microstructures with various gap distances. Menisci shape and extent of advancement are dependent on gap distance when the liquid filled channel is drained. Menisci move in the direction of fluid drainage. The menisci shape and extent of advancement are dependent on gap distance. At certain point, only the meniscus at the largest gap advance and the rest retreat.

and pressure difference between liquid and air. The curvature of the meniscus is determined by the Young-Laplace equation, which describes the pressure difference across the interface, Δp, a product of the liquid-gas surface tension γ and interface curvature κ: $\Delta p = \gamma\kappa$. The curvature of interface is given by $\kappa = {}^{1}/_{R_1} + {}^{1}/_{R_2}$ (see Figure 2.3), where R_2 can be assumed constant. The radius of curvature from a top view, R_1, must be identical for each section of the meniscus comparted by the posts because the pressure difference, Δp, should be uniform. Hence, the larger the gap between the posts, the meniscus advances further into the liquid region, increasing the dry region.

We now consider the bulging process of the meniscus in detail. Figure 2.3 illustrates the shape evolution of the meniscus as the contact line moves along the circular post surface in the direction of increasing α (angle between the center of post and the contact point of meniscus at the largest gap). A geometric consideration readily relates R to α

as $R = {(L_1 - 2r\sin\alpha)}/{(2\sin\alpha)}$, where L_1 is the largest gap between the posts and r is the radius of the post. Here the receding contact angle is taken to be zero due to the wettability of the post surface. For $0 \leq \alpha \leq \pi/2$, R decreases until it reaches $R_m = {(L_1 - 2r)}/{2}$ when $\alpha = \pi/2$. R increases afterwards, *i.e.* for $\alpha > \pi/2$. The meniscus between the posts of narrower gaps, L_2 ($L_2 < L_1$), also has the radius of curvature R when viewed from the top. This allows us to predict the location of the contact line on the posts, β in Figure 2.3, $\beta = \sin^{-1}({L_2}/{2(R+r)}) = \sin^{-1}({L_2\sin\alpha}/{L_1})$. β increases as α grows from 0 to $\pi/2$ but rather decreases with $\alpha > \pi/2$. Consequently, β cannot exceed $\pi/2$, implying that the meniscus between the posts of narrower gaps is always pinned in the region $\beta < \pi/2$.

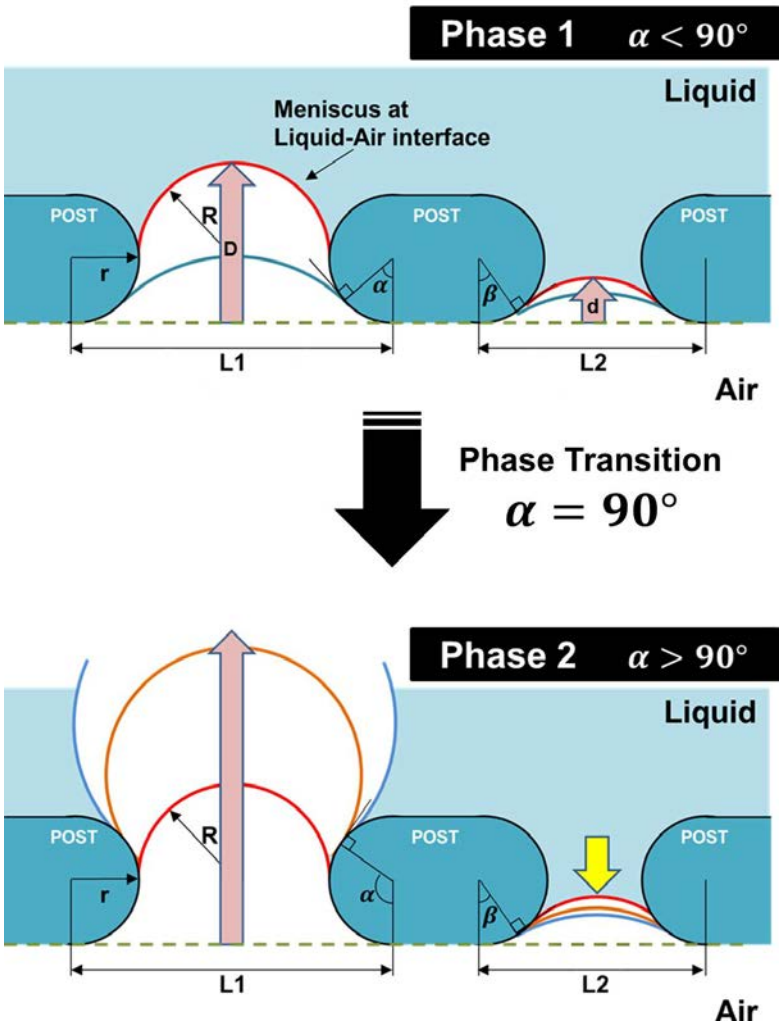

Figure 2. 3 Geometric analysis of meniscus dynamics starting from baseline (dotted line). The meniscus dynamics undergoes a transition when $\alpha = \pi/2$, (α is the angle between the center of post and the contact point of meniscus at the widest gap. In phase 1, all menisci advance toward direction of liquid drainage and the while the radii of curvature decrease. In phase 2, the meniscus at widest gap advances but all other menisci retreat toward air region while the radii of curvature increase.

Figure 2.4 (A) shows the plot of the radius of curvature and the corresponding distance between the pole and the starting line, D (Figure 2.3), for a meniscus between the post of the largest gap as a function of α. We can simply get $D = R + r - {L_1}/{(2\tan\alpha)}$. Despite nonmonotonic behavior of R with α, D increases monotonically for entire range of α. On the contrary, the advanced distance at the narrower gap, d, can be expressed as $d = R + r - {L_2}/{(2\tan\beta)}$. As the expression of d, the meniscus at narrower gap advances until $\alpha < \pi/2$ and retreats after $\alpha > \pi/2$ because β increases until $\alpha < \pi/2$ and decreases after $\alpha > \pi/2$. Figure 2.4 (B) shows the advanced distances at various gaps (D and d).

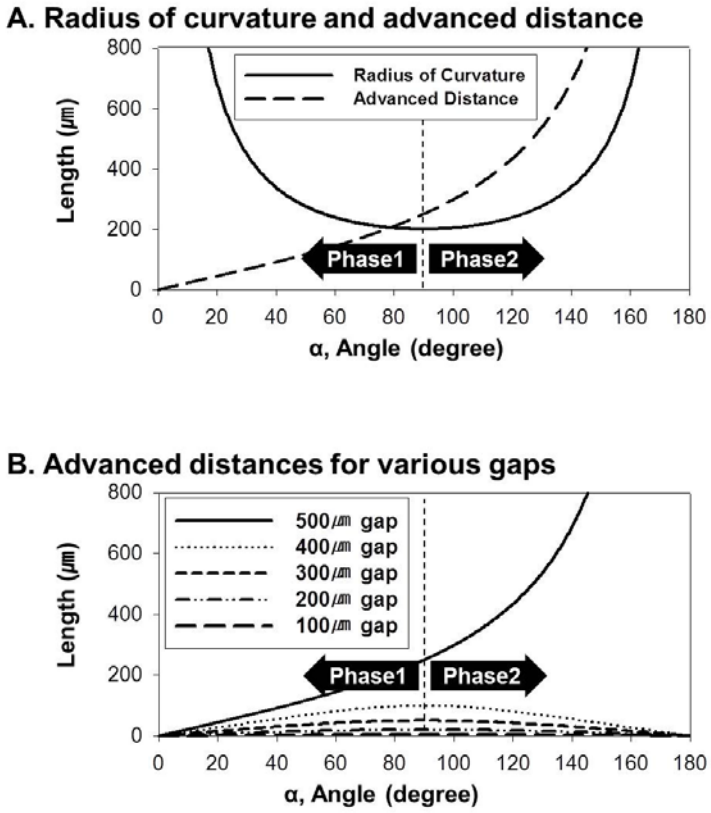

Figure 2. 4 (A) Plot of radius of curvature and meniscus advancement based on geometric analysis at the widest gap according to the angle α. The radius of curvature decreases from infinite to $(L_1 - 2r)/2$ while the angle α increases from 0 to π/2. After the transition at $\alpha = \pi/2$, the radius of curvature increases when $\alpha > \pi/2$. The advanced distance D at the widest gap increases while the angle α increases from 0° to 180°. (B) Plot of advanced distance of menisci based on the geometric analysis for various gaps. As the angle α increases 0° to 180°, meniscus at the widest gap advances but other menisci at narrower gaps advance until $\alpha < 90°$ and then they retreat after $\alpha > 90°$.

As the geometrical analysis indicates, the meniscus dynamics can be separated into two phases. In the first phase, all menisci bulge into liquid region until $\alpha < \pi/2$ but after the transition ($\alpha = \pi/2$), only the meniscus at the largest gap advances while all other menisci retreat to maintain constant radius of curvature dictated by constant Δp.

To confirm and compare the mathematical model for the shape of menisci of different gap distances, we performed experiments with gap distances from 100 μm to 400 μm between posts. Figure 2.5 shows the COMSOL simulation and experimental results, respectively, which reveal favorable agreement between theory and experiment. All menisci in the channel advance and grow during initial phase 1, shown in the first two pictures in Figure 2.5 (A) and 2.5 (B). When the radii are minimized at the transition point to phase 2 ($\alpha = \pi/2$), only the meniscus at the largest gap (400 μm) bulges while the other menisci retreat.

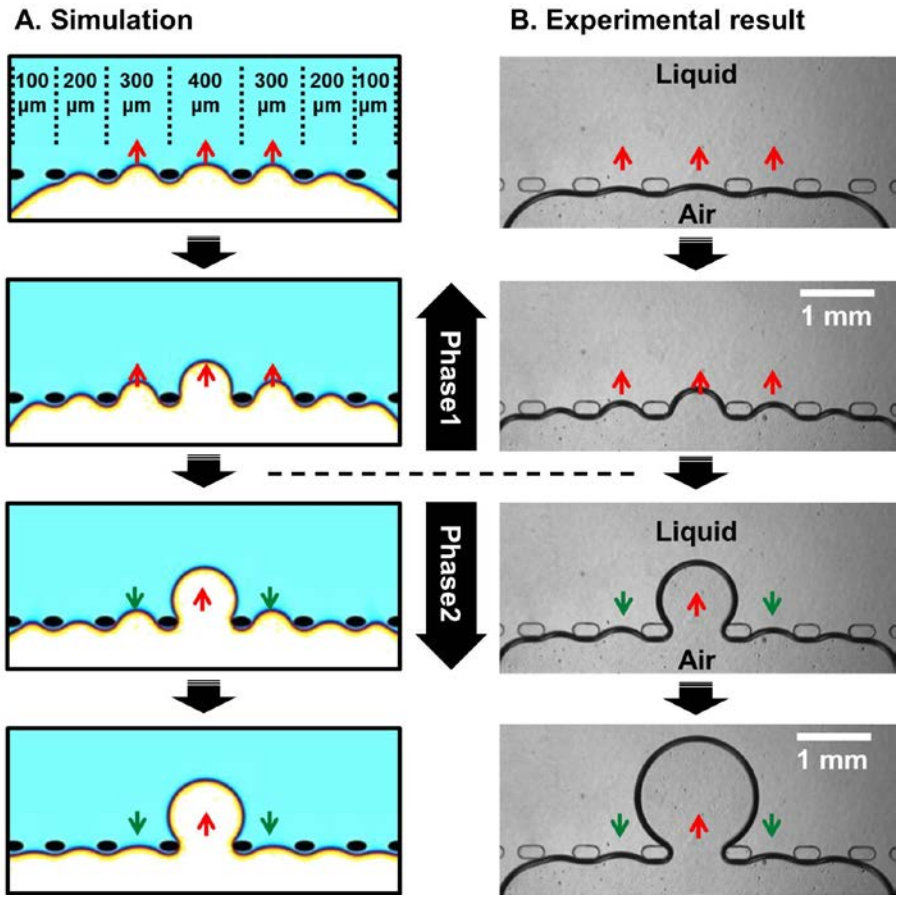

Figure 2. 5 Simulation and experimental results of meniscus dynamics. Both simulation and experimental results show two distinct phases of meniscus behavior and confirmed the analysis obtained with geometrical analysis.

2.3.2 Liquid patterning using designed post arrays

Different behaviors of menisci that straddle posts of different gaps can be exploited to trap liquid within a designated region defined by densely spaced posts. Figure 2.6 shows the corresponding liquid trapping process. A microchannel of 100 μm height initially filled with water is dried through side areas that are open to the atmosphere. The microposts are arranged in different groups so that three groups of 4 posts that are separated by 100 μm from each other. The distance between the rectangles is 500 μm. The first image shows the picture when the dewetting front meets the posts. The menisci pass through the widest gaps in the second image as explained earlier. Eventually, liquid is trapped around the group of 4 posts to result in three patterned micro-liquid islands, as shown in the third image. Because the gap between the posts are 100 μm, the trapped volume is ~1 nL. Figure 2.6 (B) shows a series

of photographs that show the dynamics of the menisci that spontaneous connect together as the meniscus from opposite sides of the microposts bulge and grow. The thin liquid film between the bulging interfaces is squeezed out of the gap, leading to the snapping of the capillary bridge. This experimental result shows same tendency and agree well with the simulation result in Figure 2.6 (C). Thus, when bulging interfaces connect with each other, array of nanoliter scale micro-liquid patterns can be generated inside the microchannels as shown in next figure.

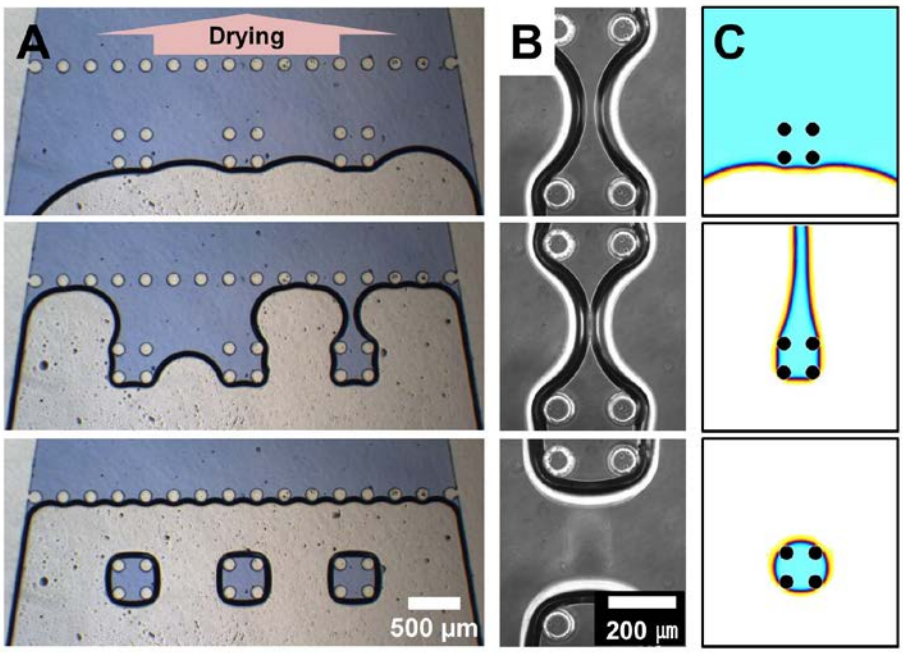

Figure 2. 6 Microliquid patterning inside microchannels. A) Groups of closely spaced posts (100 µm apart) are arrayed (500 µm apart) across the channel width (2 mm) to trap the liquid during draining. Series of photographs show advancing menisci that move around and merge, trapping 1 nL volume of microliquid between the four posts. B) Series of magnified images of the region where two menisci opposite the closely spaced posts merge. The liquid capillary between two menisci eventually breaks when the two menisci touch and snap together. C) Simulation results showing the process of capillarity guided trapping of liquid between the posts.

2.3.3 Capillarity guided patterning (CGP)

Based on meniscus dynamics via designed microposts arrays, new method for rapid liquid patterning on microfluidic platform using simple aspiration is demonstrated. Figure 2.7 and Figure 2.8 show the device design, process steps and examples of micro-liquid patterns formed by capillarity guided patterning (CGP). To generate micro-liquid patterns, liquid is first introduced into the microchannel containing the microposts array. After filling, the liquid is aspirated with bench top vacuum pump or other methods. The CGP is very robust and a variety of methods, from simple air drying to syringe pump was used to drain the channels. The CGP resulted in reproducible results over the entire microchannel. Fast removal of liquid by suction yielded identical result as the slow evaporation method. The resulting patterns were independent of the drain method and can be operated with any available equipment.

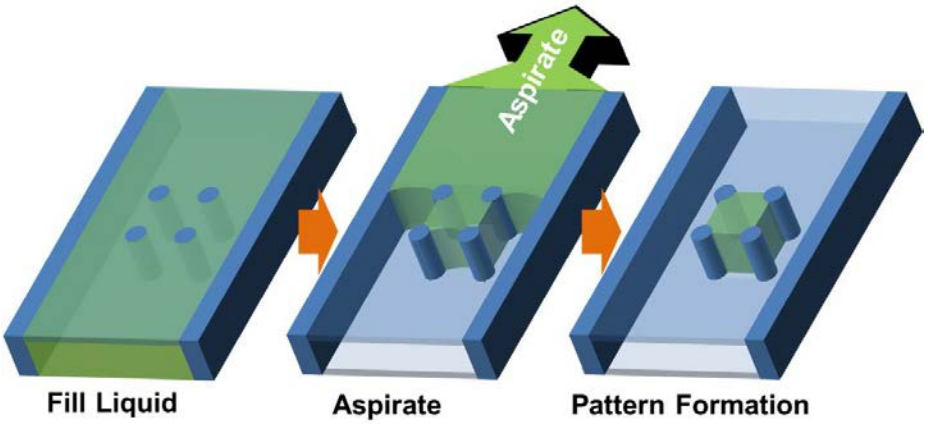

Figure 2. 7 Capillarity guided patterning of microliquid. Schematic showing the steps of CGP. A liquid filled microchannel is aspirated from one side to leave behind microliquids trapped between densely spaced posts. Simple, one-step patterning results in reproducible microliquid patterning over large areas.

Figure 2.8 shows different examples of micro-liquid patterns, from simple array of nanoliter scale micro-liquid patterns to complex patterns that fill different size patterns. The photographs show patterned nanoliter size micro-liquid (colored dye was added for visualization). The microfluidic channels were assembled from PDMS embossed channels plasma bonded to glass coverslip. The smallest post gap distance used in these examples were 100 μm and the channel height was fixed at 100 μm. Although, smaller dimensions for channel height and gaps can be fabricated and hence result in smaller micro-liquid pattern, due to ease of master mold fabrication and compatibility with extended cell culture (shown later), the minimum size was fixed at 100 μm for both the gap and channel height.

In addition to the feature size of post-post distance, an important parameter of the CGP is that for hydrophilic liquid or gel,

the channel surface has to be hydrophilic while for hydrophobic liquid, corresponding material surface should be hydrophobic. There is no constraint to the type of materials for the microfluidic device (PDMS, glass or others) or gel (i.e. matrigel or other ECM) or liquid (DI water) that can be patterned provided they have similar wettability characteristics.

After assembling the microfluidic device (surface is hydrophilic from plasma exposure), the microchannel was first filled with water. To drain the channel, a bench top vacuum pump (Δp=4.4 kPa) was used to aspirate the liquid for approximately 5 seconds. Because the pattern of trapped liquid is driven by surface tension of the moving liquid/air interface as the liquid is drained, the shape of post is not important. Various shapes can be used to generate complex features with varying sizes as long as the minimum gap between the posts is maintained. An entire device with 50 mm^2

or larger can be patterned by a single aspiration step that last only 5 seconds.

As the Figure 2.8, liquid patterns produced by CGP have irregularities in shape and size. It is caused by dirt inside microchannel and spatial pressure variation. To produce uniform liquid patterns, microchannel should be clean and the opening of microstructures (gap between microstructures) should be small and perpendicular to the flow direction (like the third image of Figure 2.8).

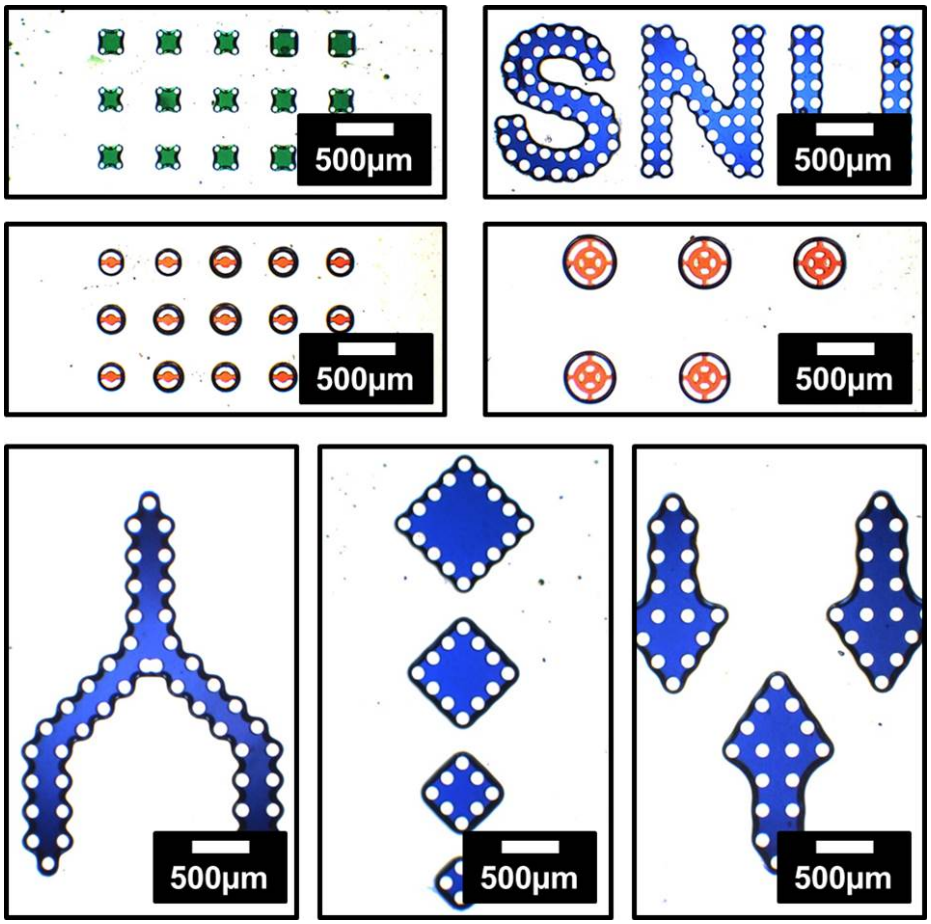

Figure 2. 8 Various nanoliter scale liquid patterns formed inside microchannel by CGP. Microliquids are trapped between densely spaced posts or structures with circular posts with small openings. Placing closely spaced structures around the boundary can produce larger patterns.

2.3.4 Maximum gap limitations of CGP

Capillarity guided patterning can produce micro-liquid patterns using a simple protocol. Unlike conventional methods where smaller patterns are more difficult to generate, the principle for CGP limits patterning of large structures (i.e. maximum gap between posts or structures). Capillarity guided patterning is based on pinning the meniscus using predefined microstructures. To apply CGP, surface tension should the dominant force compared to inertia and gravity. In most experimental conditions, effect of gravity is negligible. Since meniscus pinning is dependent on surface tension, if inertial force is more dominant than surface tension (i.e. fast flow) meniscus cannot be reliably pinned.

To find the upper and lower limit of patterns that can be produced by CGP, we analyzed the Weber number (We), a fluid

mechanical dimensionless number that provides relative importance between inertia and surface tension. When the Weber number equals to 1, inertial force and surface tension are equally operative, but when it is smaller than 1, surface tension is more dominant. To apply CGP inside microfluidic channels, Weber number should be smaller than 1 (i.e. $\mathrm{We} = \frac{\rho u^2 L}{\sigma} \ll 1$, ρ: density of fluid, u: velocity, L: post gap, σ: surface tension). Substituting the values used for the experimental conditions (ρ = 1000 kg/m^3, σ = 0.07 N/m, and u = 0.55 m/s), the maximum gap (when We=1) between posts was L = 231.4 μm. Here the characteristic liquid velocity u corresponds to the average flow velocity in a microchannel for a pressure drop of 4.4 kPa along the channel length of 2 cm.

Figure 2.9 shows the theoretical limit of maximum gap size as a function of pressure difference (ΔP) for various channel height (50-200 μm). As expected, when inertial force is increased by using

larger ΔP, maximum gap that can be used to trap micro-liquids using CGP decreases as well. When microchannel height is increased from 50 to 200 μm, the maximum gap size decreases dramatically from ~3000 μm to 15 μm. As indicated on the Figure 2.9, for 100 μm high microchannels, the maximum calculated gap size is 231.4 for ΔP (4.4 kPa used in actual experiments). The experimental verification using 100 μm high microchannel is shown in Figure 2.10. A series of patterns with gaps between 100 to 500 μm were fabricated and tested. As predicted from theoretical calculations in Figure 2.9, gaps upto 200 μm are successfully and reliably trapped by CGP. However, for patterns starting at 250 μm and above, the trapping is inconsistent and random. As discussed earlier, the maximum gap limit can be affected by properties of liquid (i.e. density, viscosity and surface tension), microchannel dimensions (i.e. length, width and height) and applied vacuum pressure. Thus when used with precise

pressure controller, various complex patterns of various sizes can be patterned using CGP.

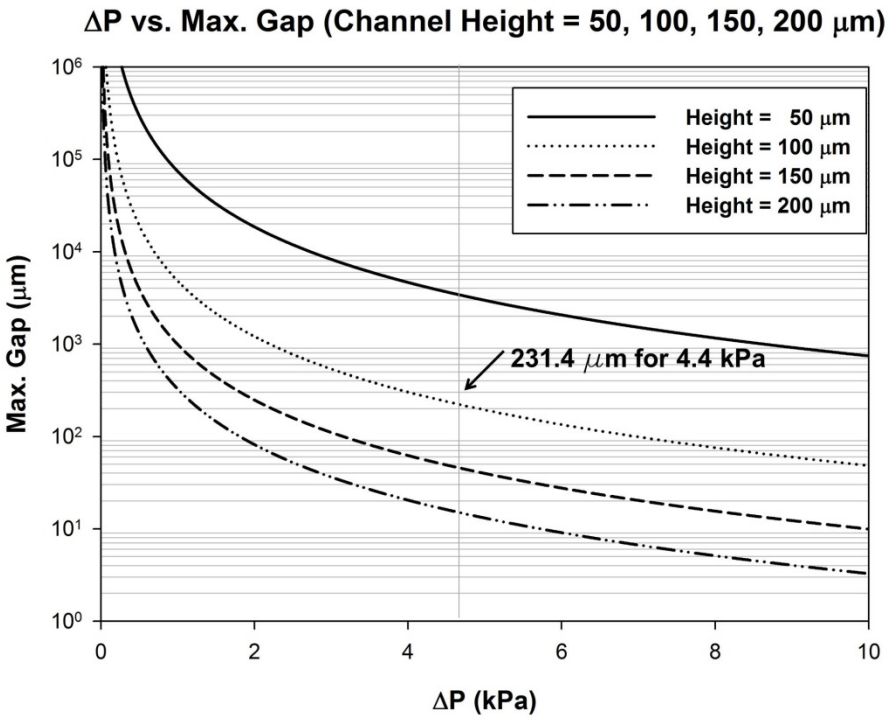

Figure 2. 9 Limitation of CGP 1: Maximum gap. Theoretical analysis of the maximum gap limit of CGP according to the pressure differences (ΔP) and channel heights. The gap limits were calculated using the Weber number which stands for the relative importance between inertia and surface tension. As a result, theoretical limit of CGP was 231.4 μm with the conditions used in this experiment (channel height = 100 μm, ΔP = 4.4 kPa).

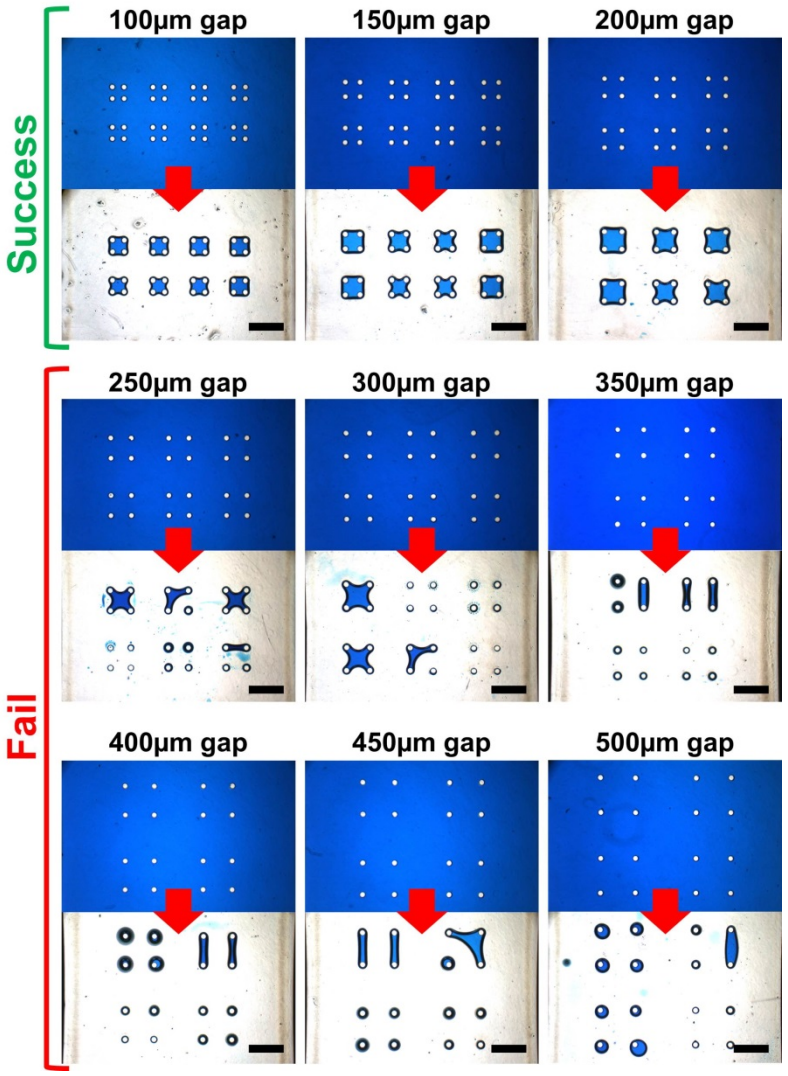

Figure 2. 10 Experimental results to find gap limit of CGP. Microliquids were successfully patterned when the gaps between two microposts were 200 μm or shorter. However, consistent with the theoretical analysis, microliquids were not patterned when the gaps were larger than 200 μm. Scale bar = 500 μm.

2.3.5 Pattern uniformity according to microstructures

Another limitation of CGP is pattern uniformity. To measure the uniformity of liquid patterns, 5 different shapes of posts were fabricated and tested. The major differences between among two 5 different designs were the ‘size of ‘opening’ and ‘direction of opening’. To compare the uniformities of each shapes, coefficient of variation (CV=Standard Deviation ⁄ Mean) was used. As the results, different shapes showed different uniformity. The CVs of each shape were 0.17, 0.19, 0.21, 0.09 and 0.15. In other words, the shape #4 (CV=0.09) showed the best uniformity among the 5 shapes. Therefore, to make well-regulated patterns, the opening of microstructures should be minimized and placed in perpendicular to the flow direction.

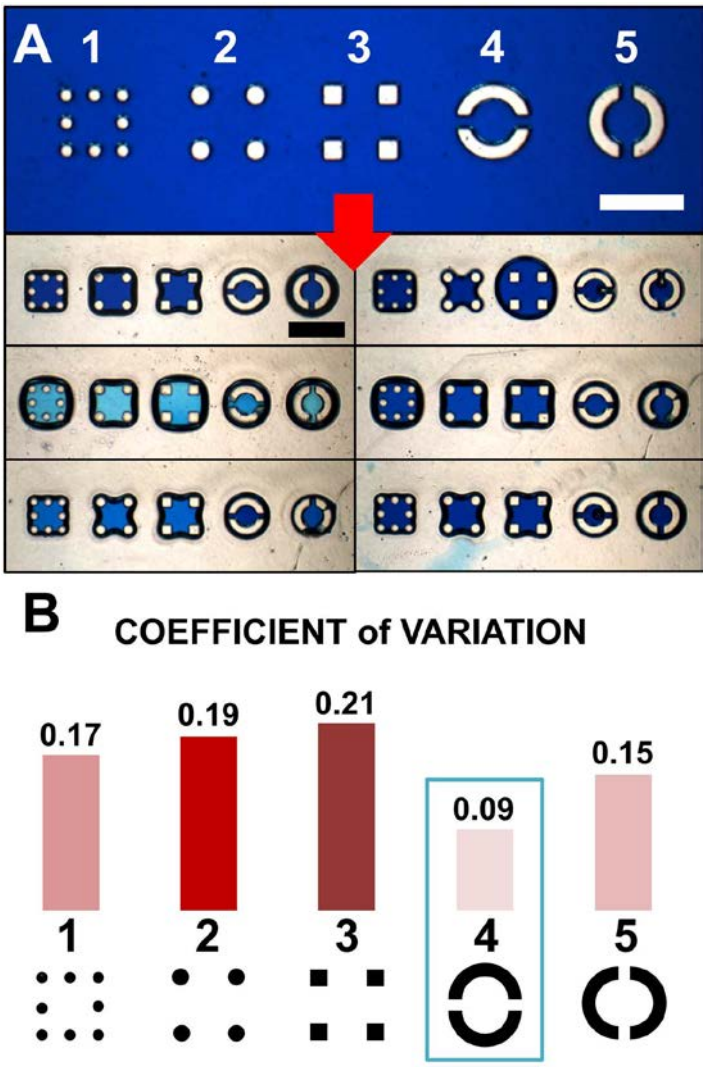

Figure 2. 11 Limitation of CGP 2: Uniformity. Liquid patterns show different uniformities due to the shape and gaps of microstructure arrays. (A) Experimental results for measuring pattern uniformity. (B) Coefficients of variation according to the various microstructure arrays. Scale bar=500 μm.

2.3.6 Patterning of multiple nested materials

Using the new CGP method, complex patterns with different materials can be patterned that are difficult to obtain with conventional photolithography or soft lithography techniques. Multiple nested materials (i.e. Russian doll-like pattern) or isolated array of small micropatterns can be readily formed as shown in Figure 2.11 and Figure 2.12. In this experiment, we used photo-curable hydrogel (PEG-DA) to visualize the shape and colors of patterns. Figure 5A shows the schematic of the fabrication process for patterning 3 different types of photo-curable hydrogels. To demonstrate the potential, we used a simple design that contained an array of posts to trap red, green, and blue labeled poly(ethylene glycol) diacrylate (PEG-DA) (UV curable polymer mixed with color ink). The post arrays are made up of groups of 4 posts (d=100 μm, gap=100 μm) that are placed in periodic array with distance of 500

μm from other groups. The width of the channel was 2 mm. Repeated steps of filling, aspiration, UV exposure are repeated to generate the patterns. For the first pattern-trapped by the group of 4 smallest posts, the channel was filled with red PEG-DA and aspirated to generate an array of ~1 nL patterns. These first patterns were used subsequently to trap the second material (green PEG-DA) with larger size features, ~25 nL. Finally, blue PEG-DA was filled into the entire channel and solidified to encapsulate the array of 2 different materials. Using the patterns generated from previous steps, multiple hierarchical structures can be patterned using this method (Figure 2.12). As shown in following sections, cell containing 3D gels can be patterned into arbitrary configuration for different biological investigations such as co-culture of cancer and HUVECs as shown in Figure 2.15.

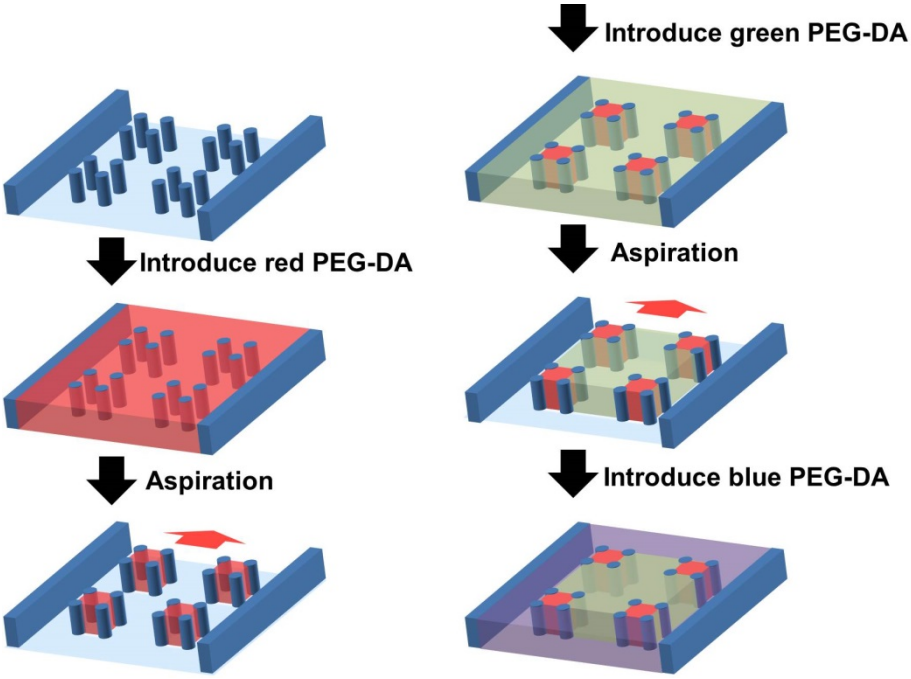

Figure 2. 12 Nested patterning of multiple materials by sequential CGP. Repeated filling and aspiration result in patterning of multiple materials. First, the channel is filled with first liquid. Perform first CGP to pattern microliquids inside densely placed post arrays (groups of four posts in the schematic). Solidify the first material (red PEG-DA) by UV exposure. These patterns act as “new posts.” Repeat second CGP to trap and solidify second material (green PEG-DA). Third material, blue-PEG-DA is filled into the rest of the channel and solidified. In this manner, multiple nested patterns can be obtained.

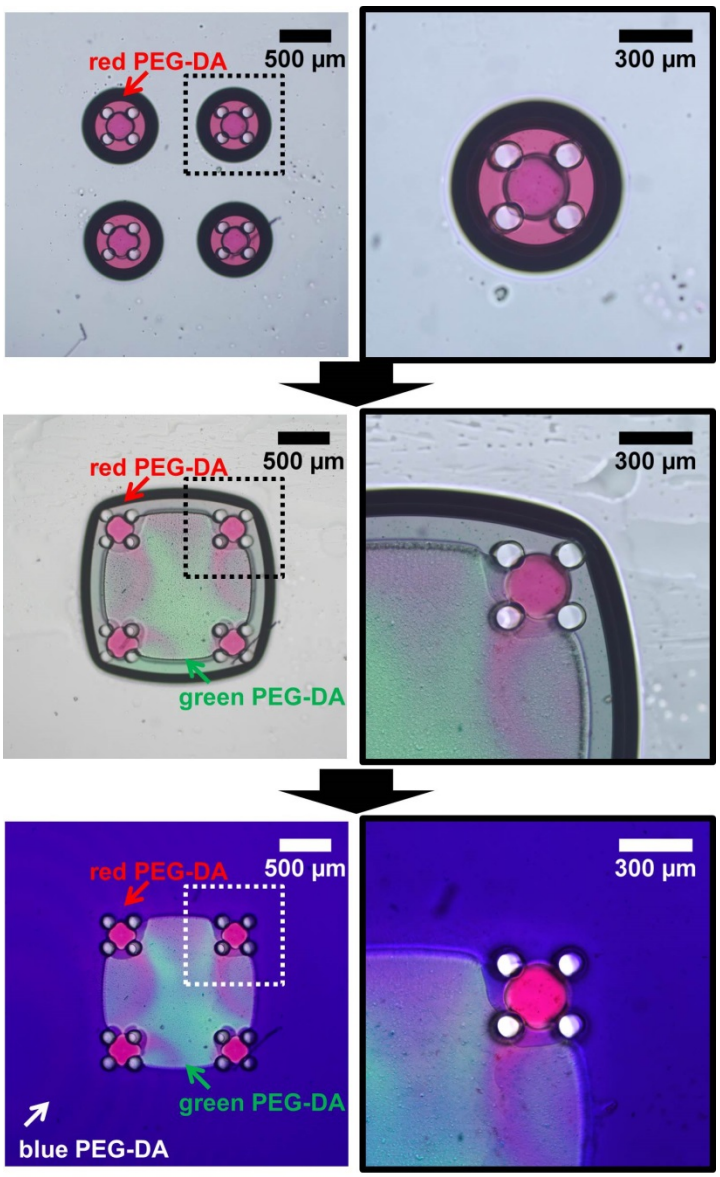

Figure 2. 13 Experimental results of multiple nested patterns. Three kinds PEG-DA (mixed with red, green, and blue ink for visualization) were successfully patterned.

2.3.7 Patterning cells in 3D ECM

We envision that the CGP will find many applications in development of biological assay systems where cells need to be patterned in an array of single cells or co-culture conditions. Figure 2.13, Figure 2.14 and Figure 2.15 show various examples that demonstrate proof of concept cellular patterns for high-throughput long-term monitoring of *Chlamydomonas reinhardtii* (Figure 2.13), formation of neuronal networks (Figure 2.14), and formation of predefined shape of blood vessel networks (Figure 2.15).

Chlamydomonas reinhardtii is model green alga that is widely studied for potential applications in sustainable biofuel research and CO_2 mitigation. Algae are usually cultured in large scale and single cell-level investigation has not been performed widely. Microfluidics is a platform where precise culture conditions

(i.e. nutrient, carbon source, pH and etc.) can be controlled precisely.

In Figure 2.13, an array of immobilized *C. reinhardtii* (~1 nL trapped volume) within alginate hydrogel is shown. Chlorophyll autofluorescence allowed imaging without additional staining. Single cells as well as groups of cells can be trapped reliably. The picture was taken after 1 day of culture. The formation of *C. reinhardtii* array was obtained in simple 2 steps similar to examples shown earlier. The liquid was replaced with *C. reinhardtii* was mixed with alginic acid and patterned by CGP. After trapping the cell containing alginic acid, calcium containing media was filled into the channel to cross-link the hydrogel. We have successfully cultured the cells for 7 days and observed proliferation inside the alginate gel. An advantage of such array of immobilized *C. Reinhardtii* is that culture conditions can be controlled dynamically or a combinatorial mixture of various nutrients, i.e. Carbon, Oxygen,

Nitrogen etc., can be exposed to the array. Also, since the position of cells is fixed, the cellular responses can be observed in real-time using optical microscopy.

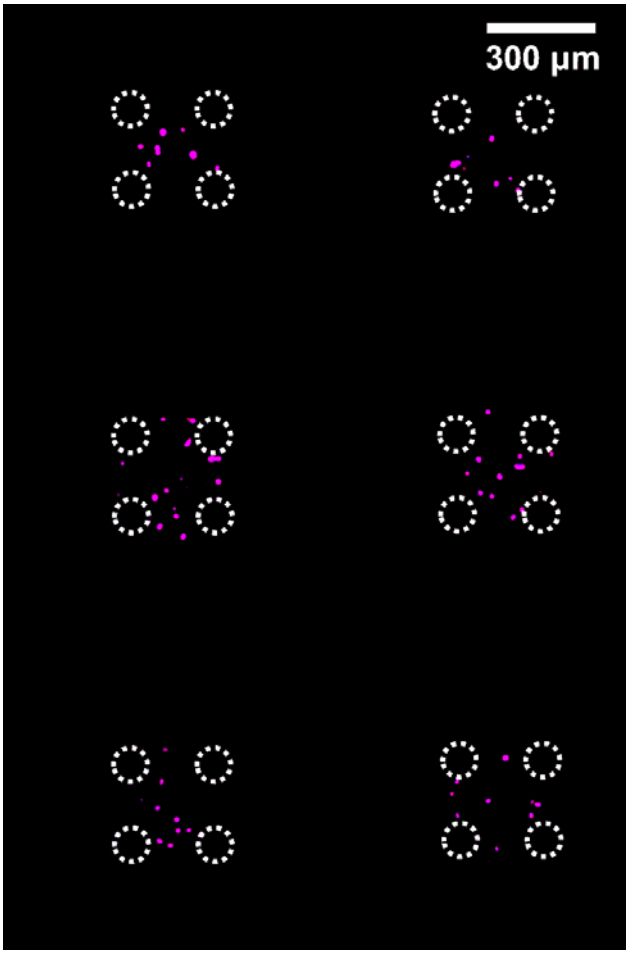

Figure 2. 14 Applications of CGP for biology: patterning cells. Isolated array of cell patterns was obtained using CGP. Microalgae, C. reinhardtii, in alginate gel (chlorophyll autofluorescence) was trapped between posts over large area. The array of cells can be used to optimize conditions for biodiesel production.

Figure 2.14 shows a photograph of neural network formed with primary rat cortical neurons. The neurons were captured in 3D matrigel matrix of artificial shape and the pattern was 2 mm long with post-post spacings of 100 μm. Primary neurons were suspended in media and equal volume of liquid matrigel was mixed immediately before filling the device. After gentle aspiration to pattern the gel, entire device was placed in an incubator to allow gelation of matrigel. Media was added after 3 min. and the culture was maintained following usual protocol. This result demonstrates that the neurons are viable (photograph was taken after 7 DIV, calcein AM viability stain) and show healthy neuritic processes. Exposure to shear stress during CGP process was not detrimental to neurons, one of the most sensitive cells to shear and culture conditions, and that the patterning process is compatible with mammalian cells.

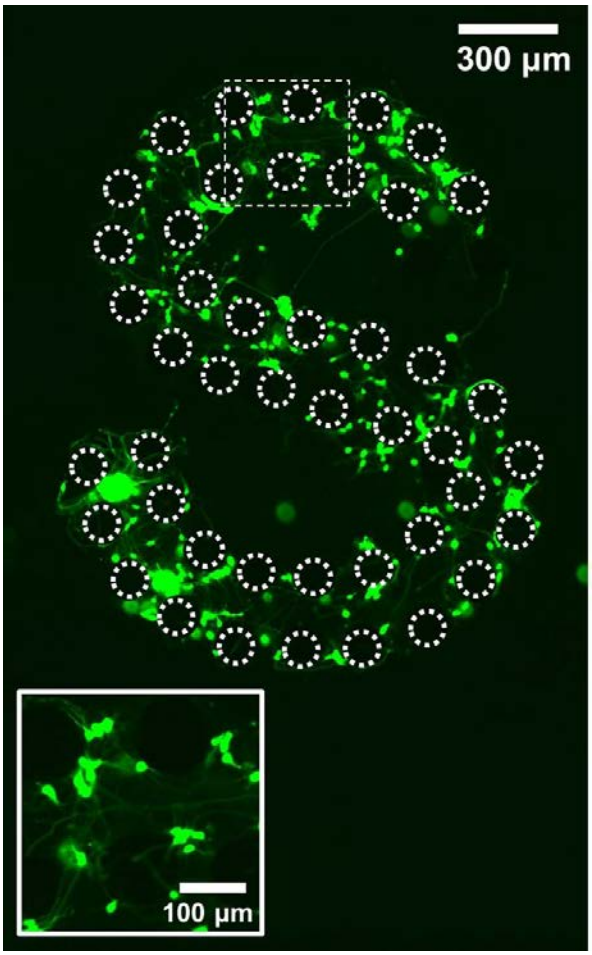

Figure 2. 15 Applications of CGP for biology: patterning cells. Designed neural network formed with primary rat cortical neurons (Calcein AM-labeled) in 3D matrigel. The neurons are healthy and show several neuritis and axons.

The fluorescent image in Figure 2.15 shows a 2 mm long Y-shaped network of blood vessel. The microchannel was first filled with HUVEC suspension in fibrinogen-thrombin mixture (liquid state, before cross-linking). Before fibrin clotted (~1 min), it was gently aspirated to leave the trapped gels behind. After cross-linking for 1 min at room temperature, the channel was filled with lung fibroblast (LF) and media. The HUVEC-LF co-culture was maintained for 5 days to allow blood vessel network formation.

The photograph shows HUVECs stained with CD31, a marker of endothelial cells (LFs were not stained for clarity). Confocal cross-section images at 3 positions along the pattern clearly show lumens formed by the HUVECs. This result illustrate that when HUVECs are patterned into arbitrary shaped gel, perfusable network can be formed that are guided by the design.

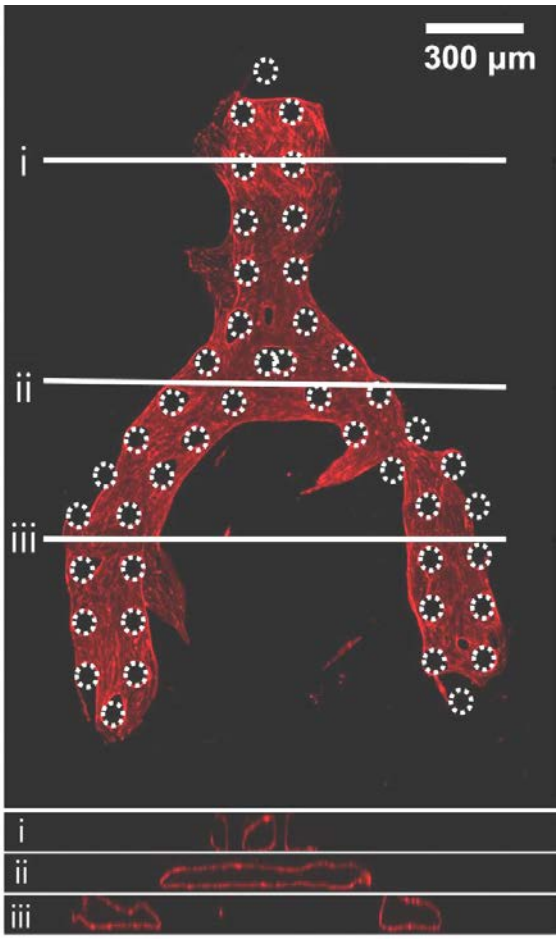

Figure 2. 16 Applications of CGP for biology: patterning cells. Engineered blood vessel with branched Y-shape. HUVECs (CD31-labeled) were mixed with fibrin gel and patterned inside designed post array.

2.3.8 Cancer angiogenesis model

Cancer cell migration and angiogenesis is a 3D process that involves cell-cell and cell-ECM interactions that are difficult to recapitulate in 2D culture platforms. Recently, several models have been developed to study these processes in 3D gels. However, none of these models can approach the simplicity of 2D experiments using a petri dish. We aimed to develop a new in-vitro model of angiogenesis that is simple and robust. Angiogenesis is a process of sprouting new blood vessel stimulated by paracrine signals from nearby cancer cells. We have patterned cancer cells and HUVECs in close proximity (less than 100 μm apart for paracrine signaling to be effective) and observed the angiogenesis toward the tumor cells.

Figure 2.16 shows the cell loading and patterning steps for cancer angiogenesis model. We have used a circular trap with 4

openings (opening size = 100 μm) to localize cancer cells (U87MG, highly angiogenic glioblastoma cells) and surrounded them with HUVECs and LFs. The channel is 100 μm high, producing 3D environment for the cells. Similar to group of 4 posts shown earlier, the circular traps are as effective in capturing U87MG cells. The shape of the structures can be designed for each application to trap different amounts/number of cells. In this case, we wished to observe the angiogenic process with time-lapse microscopy and the well-defined arrayed patterns allowed continuous imaging of a number of areas on a single chip.

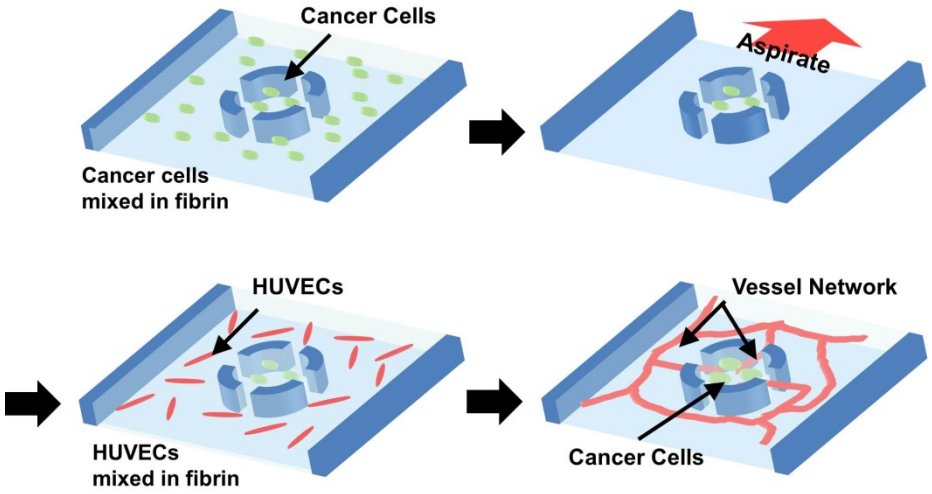

Figure 2. 17 Process for making *in vitro* model of cancer angiogenesis. Cancer cells (U87MG) and HUVECs were patterned in close proximity. This coculture model was established in three simple steps. Cancer cells were first trapped within circular areas by CGP and the rest of the channel was filled with HUVEC and LF mixture in fibrin matrix.

Figure 2.17 shows fluorescence images of area around the patterned circular trap filled with cancer cells (green GFP labeled U87MG) in fibrin. The HUVECs, placed outside the trap spontaneously form network of blood vessels after 3 days. They are clearly visible (red, CD31 stain) around the traps. By day 3, HUVEC sprouts begin to enter the circular trap area that was filled with U87MG, a glioblastoma cell line that is highly angiogenic. By day 5, somewhat dense network of vessels are visible inside the circular region as the blood vessels have penetrated the area occupied by the cancer cells. The presence of U87MG cells clearly influenced and directed sprouting angiogenesis toward themselves. These blood vessels have open lumen like the example shown in Figure 2.15.

In a simple 3-step process, a three-dimensional cancer angiogenesis model that mimic cell-cell and cell-ECM interactions

have been engineered in a microfluidic device. This model can be further developed to recapitulate the structure and organization of tumor microenvironment that is amenable to long-term observation of dynamic events such as angiogenesis and cancer cell migration during metastasis.

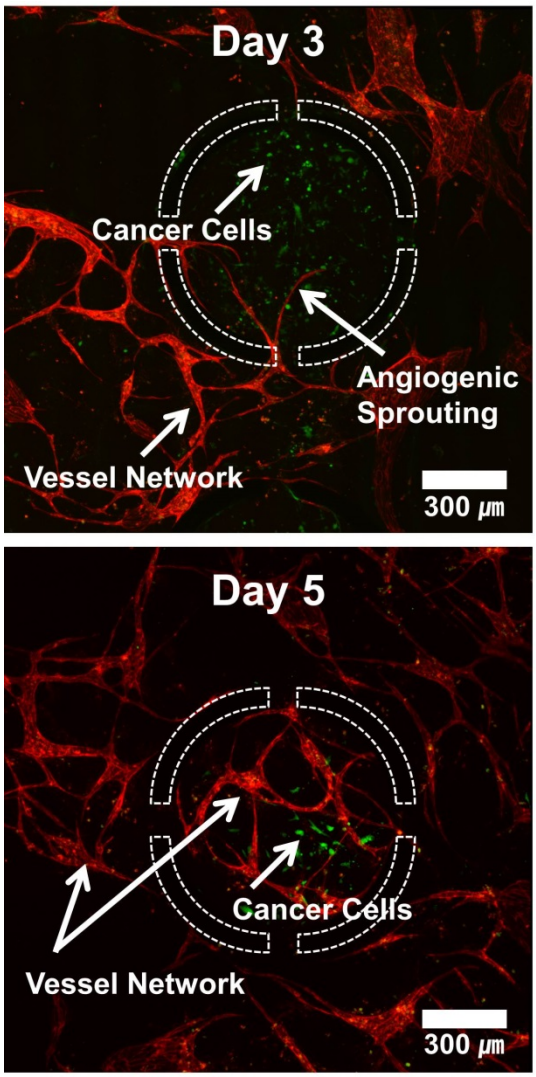

Figure 2. 18 In vitro model of cancer angiogenesis. HUVECs have formed vessel networks and some vessels have started entering the area densely populated with cancer cells 3 days after plating the cells. By day 5, numerous vessels have entered the circular cancer cell area, attracted by U87MG. The vessels have lumens and are visualized with CD31 (EC marker).

2.4 Conclusion

We developed a simple non-lithographic patterning method by engineering meniscus dynamics when a liquid filled channel is drained. When microstructures are strategically placed, surface tension-driven trapping of liquids take place as advancing menisci snap and merge, spontaneously generating isolated micro-liquids. Detailed analysis of the meniscus dynamics based on hydrodynamics resulted in understanding the factors that influence meniscus advancement during channel draining. We formulated meniscus dynamics between microstructures as a function of α (angle between the center of post and the contact point of meniscus at the largest gap) and gap distance and determined conditions where adjacent advancing menisci snap and merge around structures to trap micro-liquids. Based on this geometric analysis, arbitrary isolated micro-liquid and gel patterns were generated by strategically placed

microstructures. The capillarity guided patterning process is extremely robust, yielding reproducible patterns under variable experimental conditions. Nanoliter scale liquids or gels containing single cells can be reliably patterned over large areas. The patterning process is extremely simple and fast. Filling of the channel followed by draining (vacuum aspiration, natural drying or others) instantaneously generates patterns over the entire microfluidic device. For microchannels that are hydrophilic, water or gels instantaneously fill the entire channel (even for circular traps with small openings i.e. Figure 3B and Figure 8). Application of vacuum aspiration at one end of the channel is all that is needed to obtain the patterns. One step of CGP takes less than 5 seconds to generate the patterns.

A novel patterning method based on fluid dynamics is described and also the limitations of the method are analyzed both

theoretically and experimentally. Capillarity guided patterning was used to trap single cells or groups of different cells (for co-culture) to build an in-vitro platform for on chip drug screening and organ-on-a-chip applications. We believe that the simplicity and robustness of the method will be attractive for a number of biological experimental platforms that involve engineering 3D cell microenvironment.

Chapter 3.

Capillarity Guided Patterning of Microliquids on Large Surface

3.1 Introduction

Handling and analyzing of microliquids with cells take an important role in biomedical engineering, especially drug screening. [31, 39] More than half of all drug screening processes are cell based assays. [39, 66, 67] Conventional drug screening assays have been performed within petri dishes or multiwell plates for its convenience of handling and accessibility. [36, 37, 68, 69] However, this conventional tool has critical disadvantages; consumption of materials, cells and reagents. To overcome these problems, a lot of researchers started getting interested in microfluidics. [70-73] Microfluidics offers a lot

of advantages for handling liquid; lower consumption of materials and reagents, fast reaction and multiple functions. [18, 25, 28, 40, 74]

Development of microfluidics has led a lot of biomedical applications such as Lab-on-a-chip and Organ-on-a-chip. [12, 45, 75] Also microscale patterning methods have been developed for high-throughput screening. Recently, there are many patterning methods using hydrogels, UV curable materials, droplets, optical twizzers and microwells. [21, 35, 76-78] Among those patterning methods, microwell-based patterning method is the most widely used technique to immobilize cells at the designated positions for high-throughput screening. Microwell-based patterning method can make many patterns by using simple liquid drawing motion in short time. [37, 39, 79-81] Also the microwell-based method can be applied to both inside and outside of microchannels. However, microwell-based method requires surface modification such as oxygen plasma treatment for

making hydrophilic surfaces. Also the imaging of patterned materials by microwell-based method is limited because of the relatively thick substrates. [17, 82-89]

In this chapter, we introduce a new liquid patterning method on large surface by simple wiping motion using embossed microstructures. This method is similar to the capillarity guided patterning in microchannels mentioned in previous chapter but this method can be applied outside of microchannels. Using this new technique, we demonstrated variety liquid patterns containing cells on large surfaces. The microscturture embossed substrates were fabricated by solvent assisted molding. Furthermore, we introduce a sample collecting method. Compared to other patterning methods, this new patterning is: (i) simple and fast, (ii) robust and reliable, (iii) flexible in terms of possible pattern shape and size, (iv) no need for special equipment or surface modifications (i.e. Hydrophilization),

and (v) scalable to large area patterning.

3.2 Materials and methods

3.2.1 PDMS mold fabrication

PDMS molds for fabricating microstructures patterned polystyrene dish were fabricated using soft lithography. Master molds for soft lithography were fabricated by photolithography. SU-8-100, negative tone photoresist, was spin coated on silicon wafer with 1,300 rpm for 75 μm thickness. The coated silicon wafer was baked on the 95℃ hotplate to rid solvent inside photoresist. After baking, photomask was placed on the coated silicon wafer and exposed to UV for crosslinking.

After fabricating master mold, positive replicas with engraved microstructures were fabricated by softlithography using polydimethylsiloxane (PDMS; Sylgard 184, Dow Corning, Midland, MI) against the master mold. The PDMS prepolymer was mixed

with curing agent by 10:1(w/w) ratio. The PDMS poured master was placed inside vacuum chamber for degasing and was moved on hot plate (95℃) for curing. Cured PDMS was then separated from master mold and trimmed.

3.2.2 Solvent assisted molding

Microstructures patterned polystyrene dish was fabricated by solvent assisted molding. Specific processes are following. PDMS mold was prepared by softlithography. The PDMS mold contains engraved microstructures. After mold preparation, solvent (AZ 1500 Thinner, AZ Electronic Materials Korea, KR) was poured on PDMS mold. Then put the solvent coated PDMS in vacuum chamber for 1 minute to fill engraved microstructures with solvent. After degasing, PDMS mold was placed on the polystyrene plate

(Petri dish, SPL Life Sciences, KR). At this step, placing of PDMS mold should be gentle to prevent air bubble trapping between PDMS and polystyrene plate. From this step, polystyrene plate started dissolving by solvent. Mold and polystyrene plate was placed on 50℃ hotplate and pressure was applied on the PDMS mold with 0.2 N/cm^2. While the PDMS mold and polystyrene plate being heated, solvent inside engraved microstructures was dissipated through PDMS, because PDMS is air porous material. After 20 minutes, the PDMS mold was removed and microstructure embossed polystyrene plate was washed with ethanol. (Figure 3.1)

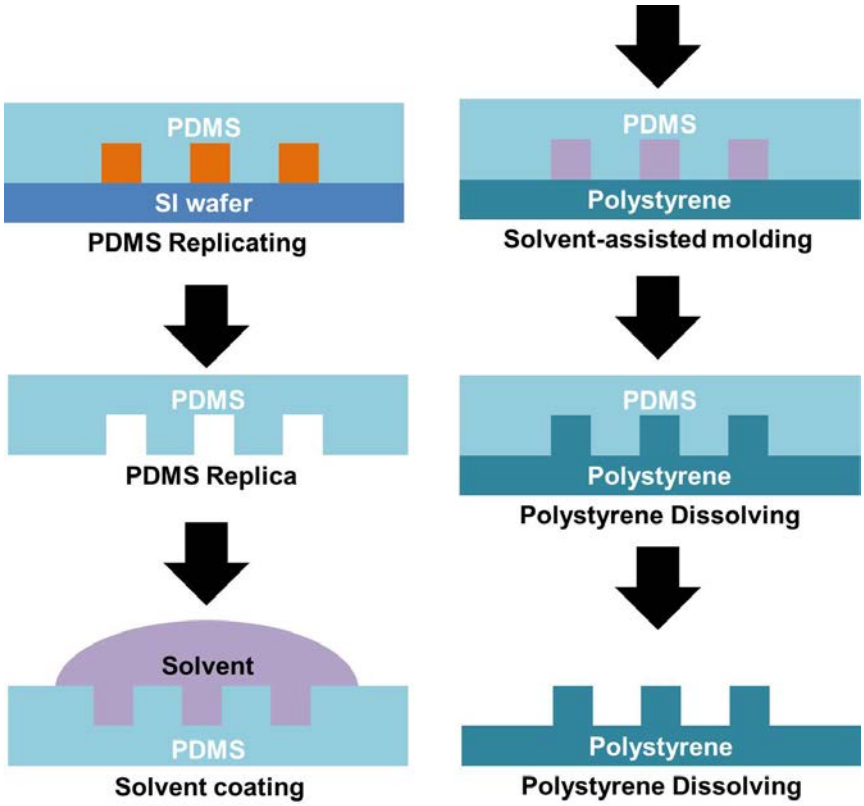

Figure 3. 1 Process of solvent-assisted molding

3.2.3 Cell culture

Chlamydomonas reinhardtii (CC-503) in tris acetate phosphate (TAP) medium were cultured at 23 °C and 5% CO_2 while shaking on an orbital shaker at 125 rpm. The cultures were exposed to 12 h cycles of light (40 μmol/s m^2) and dark.

3.2.4 Cell loading

Chlamydomonas reinhardtii suspension was mixed in 1:1 ratio with alginate solution (8%, w/v) with final concentration 5×10^6 cells/mL. The cell/alginate mixture was patterned inside micropost arrays by wiping capillarity guided patterning. Alginate gel was polymerized by introducing culture medium containing $CaCl_2$ (10%, w/v).

3.2.5 Sample collecting

The patterned *Chlamydomonas reinhardtii* mixed with alginate gel was collected by Sodium Citrate (1%, w/w, in TAP medium). Specific procedure is following. Culture medium was completely aspirated. 5 μL of TAP medium containing Sodium Citrate was put on patterned alginate gel with cells then crosslinked alginate gel was dissolved by Sodium Citrate. After 5 seconds, patterned sample can be collected by pipette.

3.2.6 Immunostaining

To image *Chlamydomonas reinhardtii*, auto-fluorescence signal from chlorophyll was used. Neutral lipid accumulated inside the *Chlamydomonas reinhardtii* was visualized by fluorescence labeling with BODIPY.

3.2.7 Imaging

Olympus FV1000 confocal microscope was used for 3D cross-sectional imaging. Images were analyzed with imageJ and IMARIS (Bitplane, Switzerland).

3.3 Results

3.3.1 Meniscus dynamics with microstructures in 3D

In the Chapter 2, we discussed about meniscus dynamics with microstructures inside microchannel according to liquid draining motion. Here in Chapter 3, we considered meniscus dynamics in 3 dimensions. Figure 3.2 (A) shows the experimental setup for observing meniscus dynamics in 3D. The microstructures embossed polystyrene plate was fabricated by solvent assisted molding (Figure 3.1). The shape of microstructures were group of 4 circular posts (diameter = 100 μm, height = 75 μm). To observe meniscus dynamics, 100 mL of water mixed with blue dye was dropped on the polystyrene plate near the post array. Then the liquid was wiped through the post array using PDMS block. Figure 3.2 (B) and Figure 3.3 (B) illustrate the meniscus dynamics during the liquid

movement. As the figures, liquid dynamics can be divided into two phases, liquid imbibition and liquid isolation.

In Phase 1, liquid meniscus met the posts array, and the liquid couldn't penetrate into the post array but the contact line moved along the post surface because the surface was hydrophobic. However, as the side view of Figure 3.2 (B), liquid meniscus at z-axis was advanced as well as the menisci of x- and y-axis. Therefore, liquid could penetrate into the post array even the surface was hydrophobic. On the other hand, if the surface and posts were hydrophilic, liquid could penetrate into the post array easily by capillary imbibition.

In phase 2, liquid was still moving by the wiping motion. In contrast with phase 1, the meniscus dynamics can be simplified as 2D motion because the liquid film was thin and flat. This being so,

the meniscus dynamics of phase 2 was almost same as the meniscus dynamics of Figure 2.6 (A) in Chapter 2.

Figure 3.4 shows the experimental results of meniscus dynamics with microstructures on 3D surface. As the figure, the meniscus dynamics was divided into two phases and the liquid was successfully patterned as expected in Figure 3.2 and Figure 3.3.

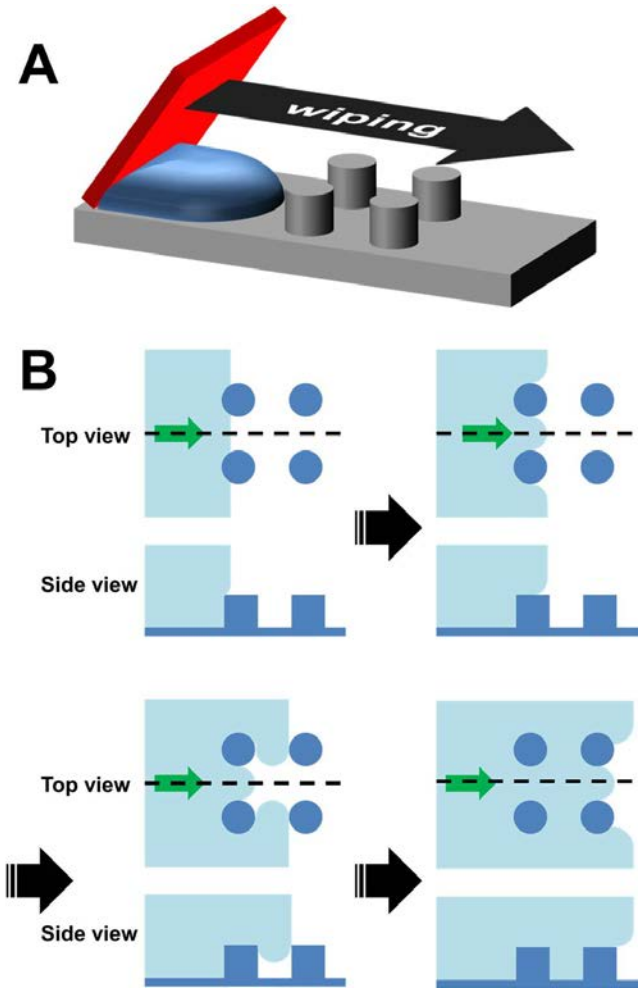

Figure 3. 2 Meniscus dynamics with microstructures in 3D: Phase 1, liquid imbibition. (A) Experimental setup for observing meniscus dynamics during liquid wiping on hydrophobic surface containing embossed microstructures. (B) Schema of meniscus dynamics and imbibition of liquid according to the liquid movement.

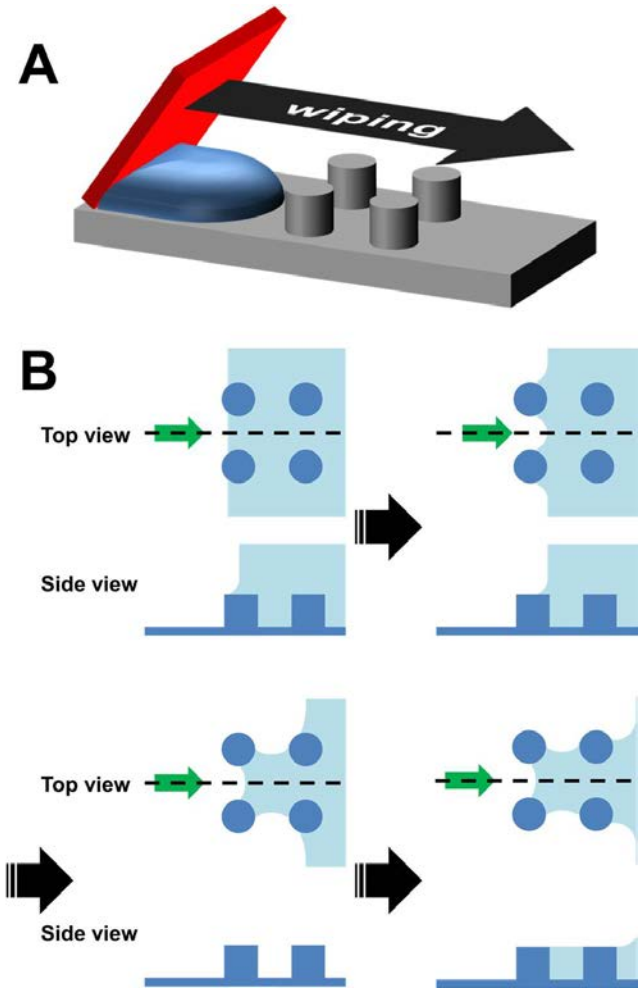

Figure 3. 3 Meniscus dynamics with microstructures in 3D: Phase 2, liquid isolation. (A) Experimental setup for observing meniscus dynamics during liquid wiping on hydrophobic surface containing embossed microstructures. (B) Schema of meniscus dynamics and isolation of liquid according to the liquid movement.

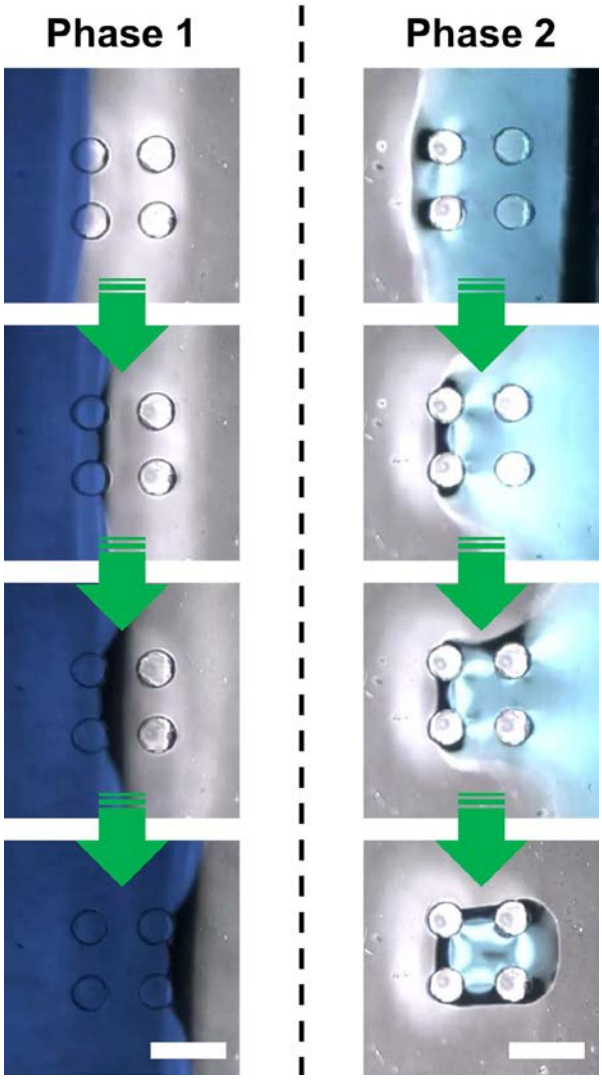

Figure 3. 4 Experimental results of meniscus dynamics with microstructures in 3D. As shown in Figure 3.2 and 3.3, meniscus dynamics process can be divided into two phases; liquid imbibition and liquid isolation. Through the two phases, microliquid was successfully patterned inside four microposts on 3D surface. Scale bar = 200 μm.

3.3.2 Capillarity guided patterning on large surface

Based on meniscus dynamics with strategically coordinated microstructures, a new method for patterning microliquids on large surface was developed. Figure 3.5 illustrates the procedure of capillarity guided patterning on large surface using liquid wiping. Procedure of this new method is quite simple. To generate microliquids patterns on surface, liquid is dropped on the target surface. The target surface contains embossed micropost arrays for liquid trapping. Figure 3.6 shows the polystyrene plate contains microstructures for liquid trapping. Then the dropped liquid is moved through the micropost arrays by simple wiping motion. Liquid wiping is done with soft material, PDMS block. During the wiping motion, liquid is trapped inside the micropost arrays and liquid patterns are generated within few seconds on large surface.

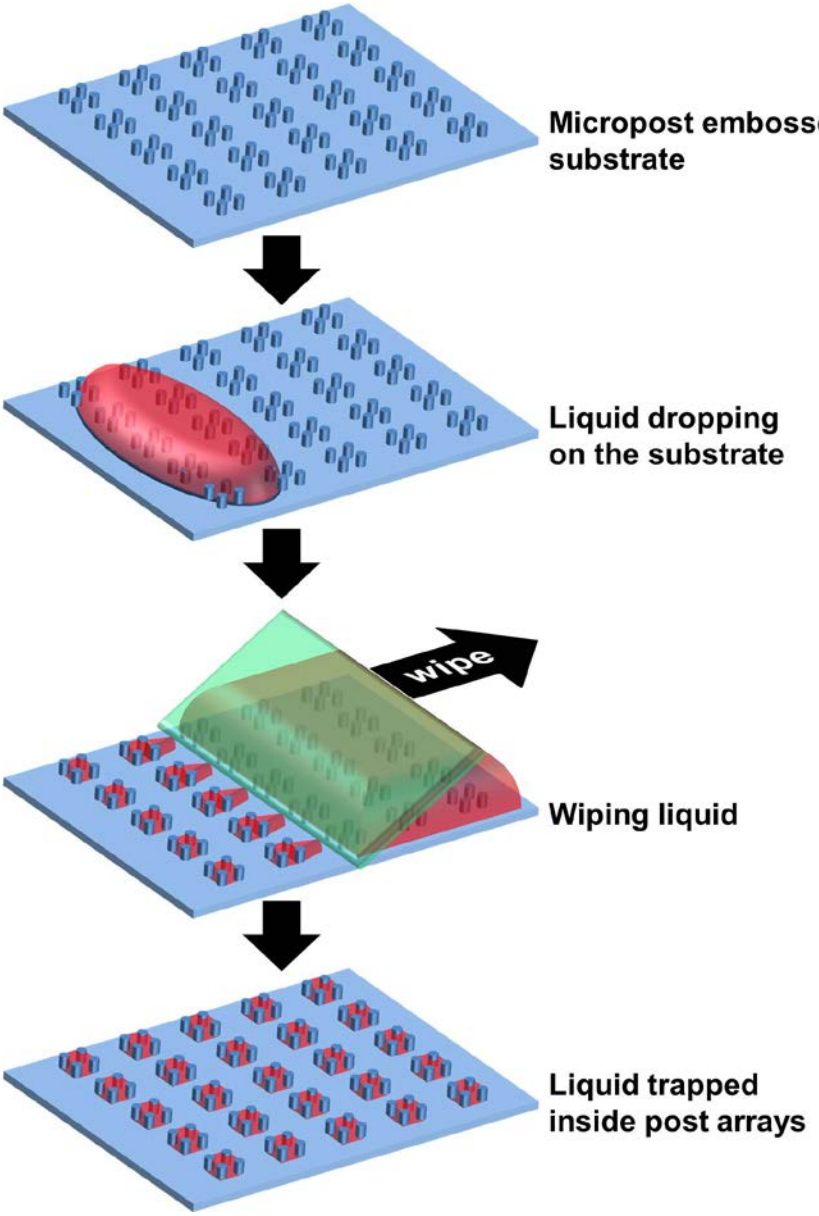

Figure 3. 5 Capillarity guided patterning on large surface.

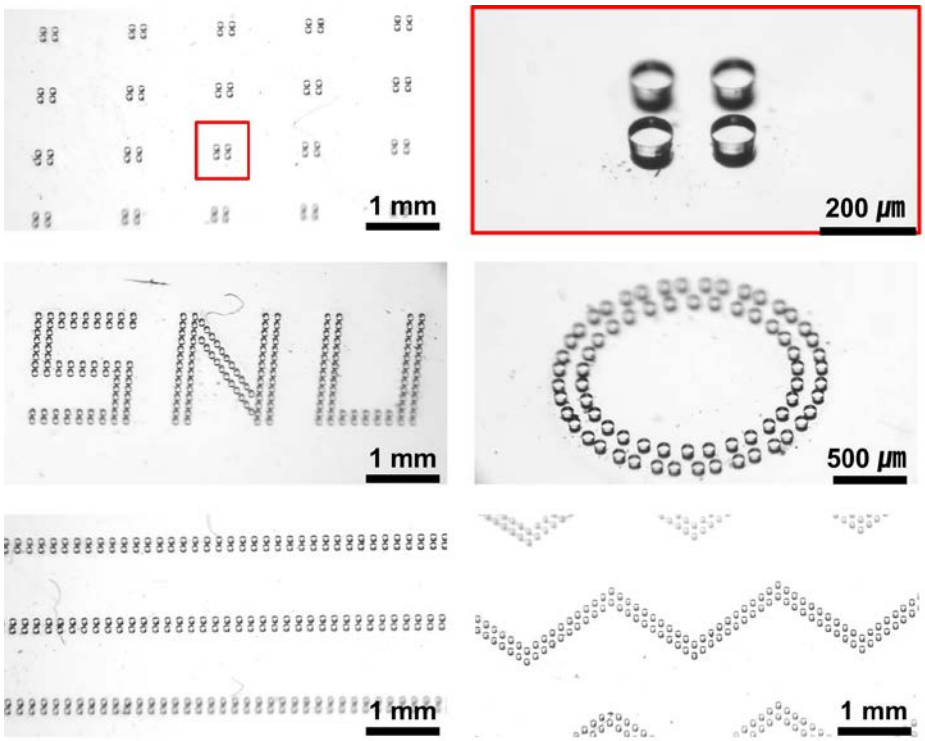

Figure 3. 6　Polystyrene plates with embossed microstructures.

Figure 3.7 shows various liquid patterns on the microstructures embossed surface generated by liquid wiping. As the Figure 3.7, liquid wiping method successfully generated various liquid patterns in shape and size. The most outstanding advantage of the wiping method compared to the aspiration method in microchannel mentioned in Chpater 2 is that it is possible to directly apply to large surface. Figure 3.8 is photograph of 8,000 liquid patterns on large surface (50 mm X 50 mm) generated by wiping method. Also, the shape of micropost was not limited in circular type. Rectangular or crescentic posts can be used for liquid trapping (Figure 3.8).

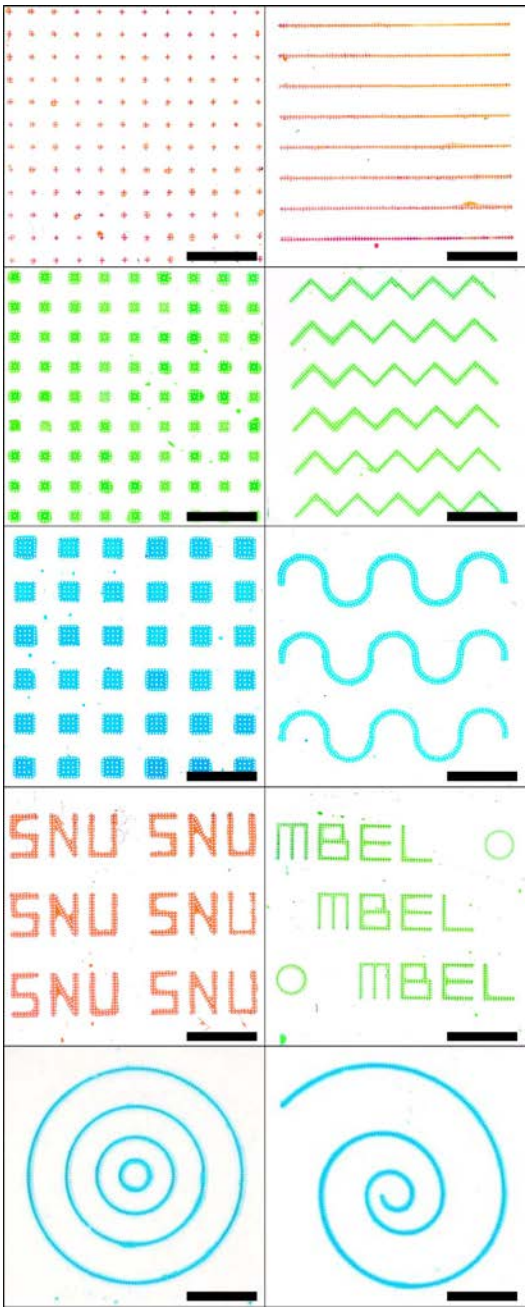

Figure 3. 7 Liquid patterns on mictructures embossed surface generated by wiping. Scale bar = 5 mm.

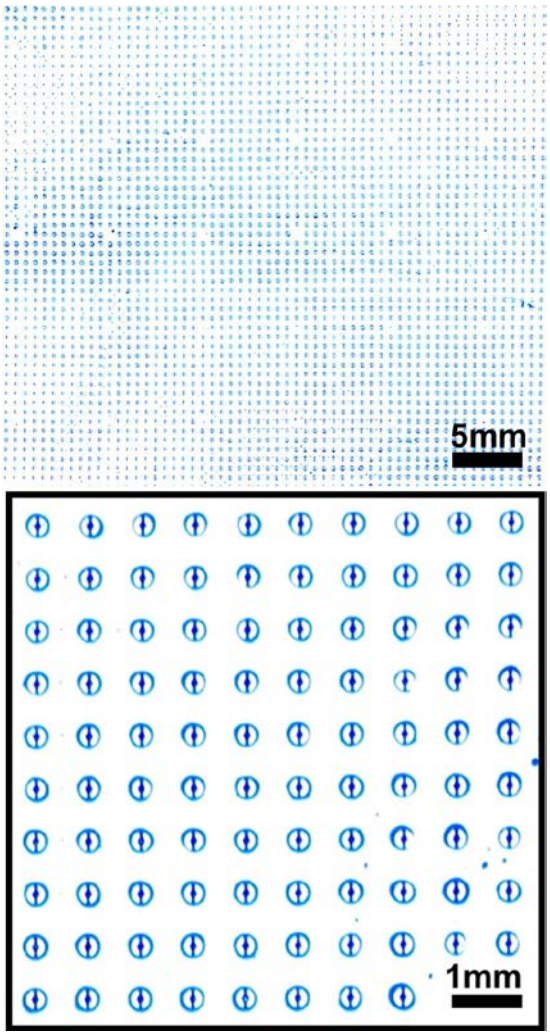

Figure 3. 8 8,000 liquid patterns on large surface made by CGP.

3.3.3 CGP vs. microwell-based liquid patterning

As mentioned before, liquid patterning is very fascinating topic in biological and chemical research area. Quite a number of researchers have been investigating on this topic, as a result, many achievements have been derived. Microwell based liquid patterning method is the simplest but effective technique among a lot of patterning methods. (REF) Microwell based liquid patterning method is quite similar to CGP; (1) both methods use microstructures on the surface and (2) both methods use wiping to spread and fill liquid inside microstructures.

To compare CGP and microwell based patterning method, various PDMS plates which contain embossed microstrictures for CGP and engraved microstructures for microwell were fabricated. The PDMS plates didn't have any treatment so the surface of PDMS

plate was hydrophobic. Figure 3.9 illustrates the experimental setup to make liquid patterns using CGP and microwell based patterning. To generate liquid patterns, liquid was dropped on the surface of fabricated PDMS and was wiped with bare PDMS block.

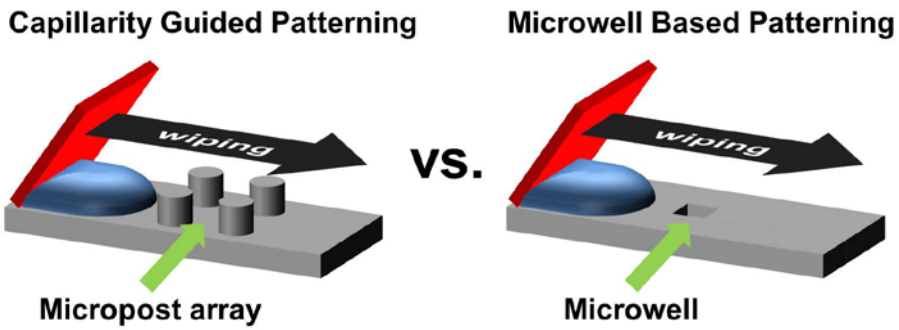

Figure 3. 9 Comparison of CGP and microwell based liquid patterning.

After liquid wiping, two PDMS plates showed different results. Figure 3.10 and Figure 3.11 show the liquid patterns generated by CGP and microwell. The efficiency of CGP was directly proportional to the post height and inversely proportional to the size of post arrays. However, the efficiency of microwell was directly proportional to the size of microwell and inversely proportional to the depth of microwell. In other words, CGP was advantageous for high aspect ratio liquid patterns and microwell was advantageous for low aspect ratio liquid patterns. (Figure 3.12)

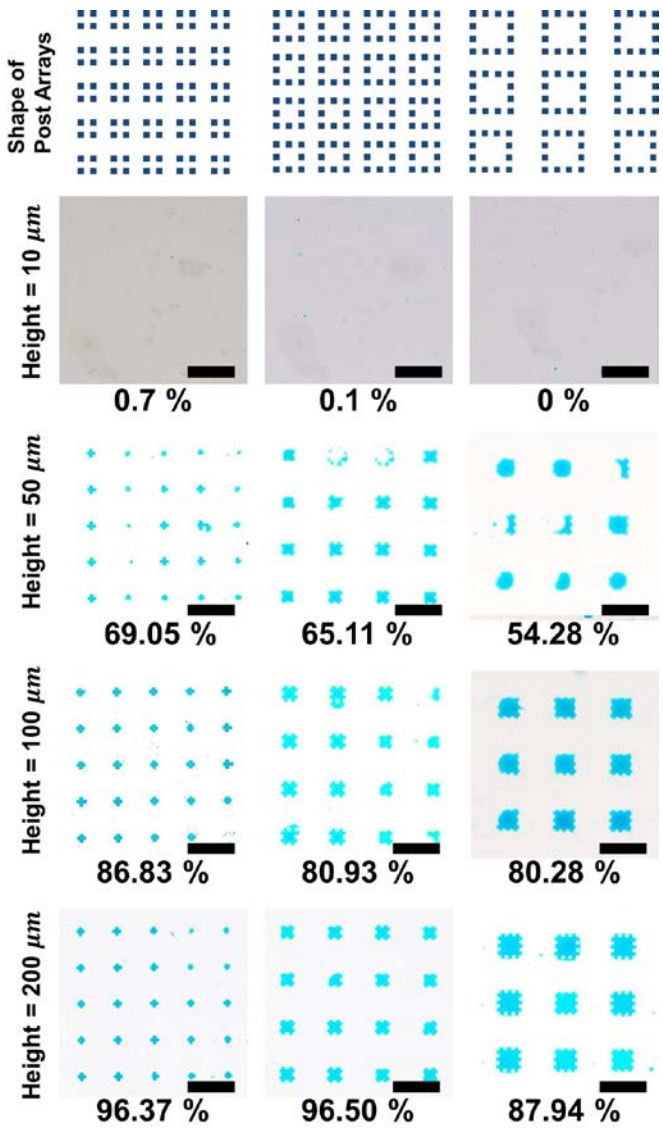

Figure 3. 10 Liquid patterns generated by CGP according to the various heights and sizes. Scale bar = 2 mm.

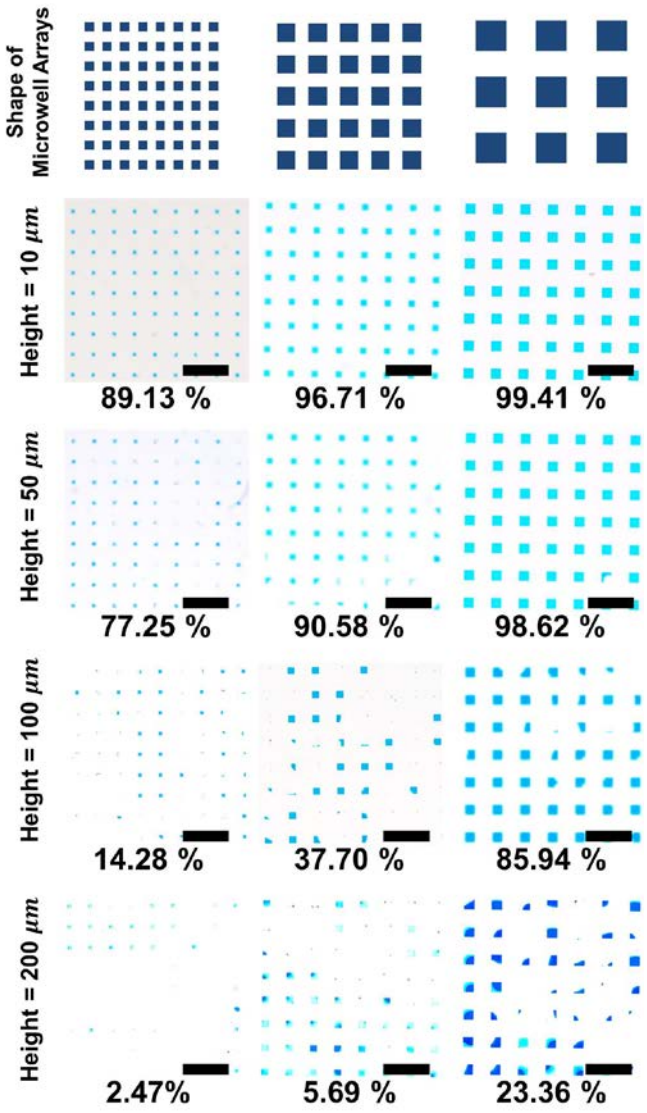

Figure 3. 11 Liquid patterns generated by microwell according to the various depths and sizes. Scale bar = 2 mm.

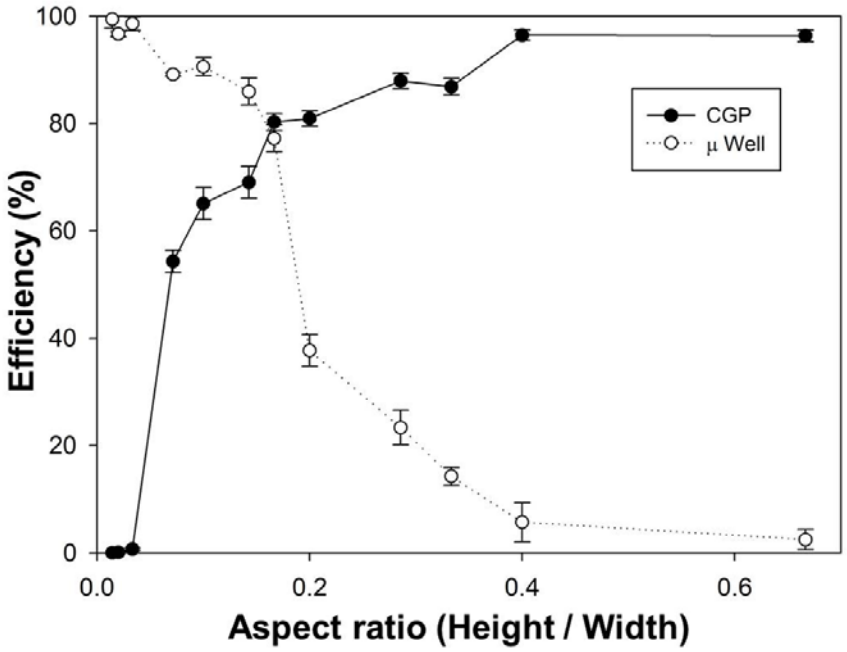

Figure 3. 12 Patterning efficiency of CGP and microwell.

3.3.4 Patterning cells in 3D ECM

As an application of CGP on large surface, we patterned *Chlamydomonas reinhardtii*, the model green alga. Green alga including C. reinhardtii is widely studied species for alternative energy source, biofuel. In this study, we patterned C. reinhardtii mixed with alginate gel for an application of CGP on large surface.

Figure 3.13 is fluorescent image which shows the patterned alginate gel mixed with cells. As the figure, alginate gel and cells were successfully patterned inside post arrays.

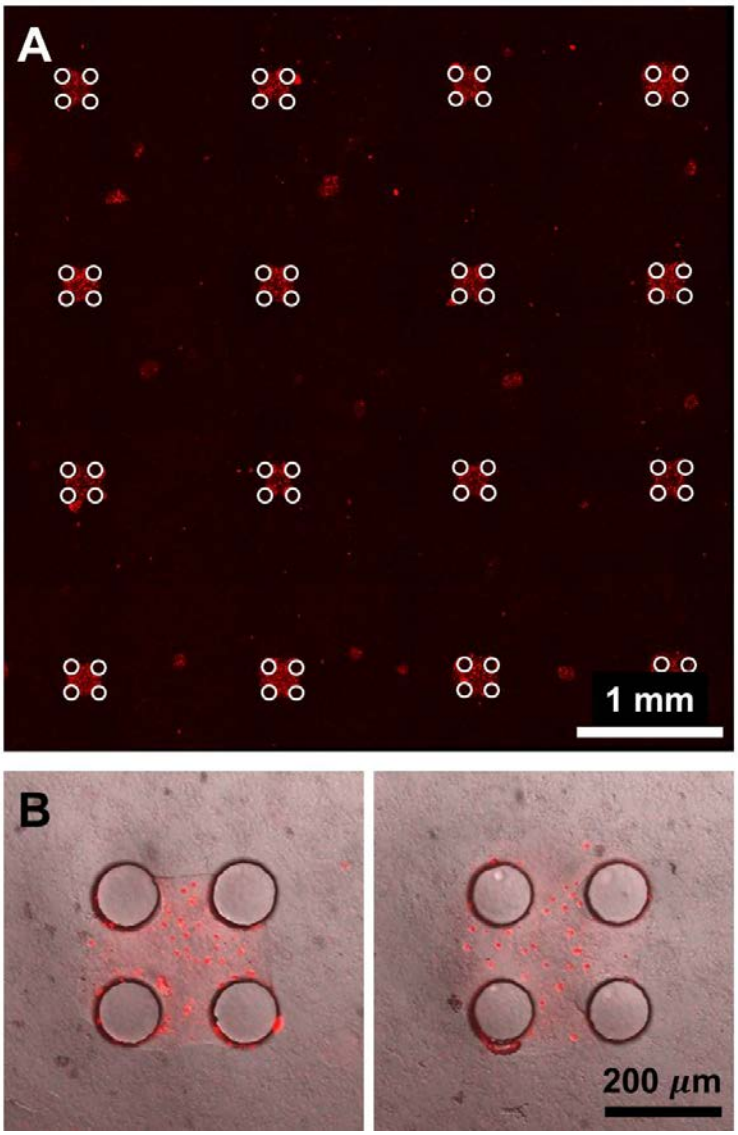

Figure 3. 13 Patterned cells mixed with hydrogel inside post arrays.

3.3.5 Patterned sample collection

High-throughput screening (HTS) is an important issue in bio-medical research field. Microfluidic devices are very attractive tools for HTS by their advantageous characteristics; small amount of cells and reagent, fast reaction, design flexibility and parallelized experiments. However, most microfluidic devices are using microstructures inside microchannel, so it is difficult to collect samples.

To overcome this problem, we applied CGP on large surface for HTS. Figure 3.14 shows the sample collecting method. The process is quiet simple, liquid patterning by wiping and collecting sample using pipette by hands. Figure 3.15 shows the design of device. The sample collecting device contains Figure 3.15 shows the design of device. The sample collecting device contains

x-, y-coordinates and position indicators to provide exact position of samples both microscopically and macroscopically. The height of coordinate structures was 5 μm to prevent sample patterning on the coordinate structures.

Figure 3.16 shows the results of sample collecting. In this experiment, sample was starved *C. reinhardtii* stained with BODIPY immobilized in alginate gel. To collect sample, 5 μL of Sodium citrate solution (10 %, w/w, in TAP media) was dropped on the sample region to dissolve alginate gel and the sample was collected using pipette.

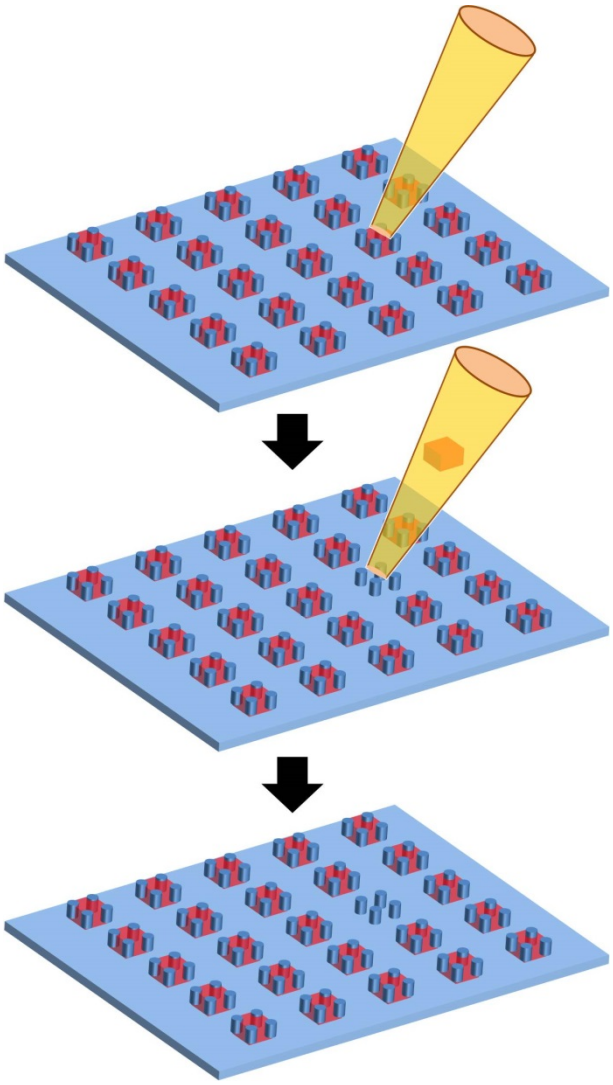

Figure 3. 14 Sample collecting method.

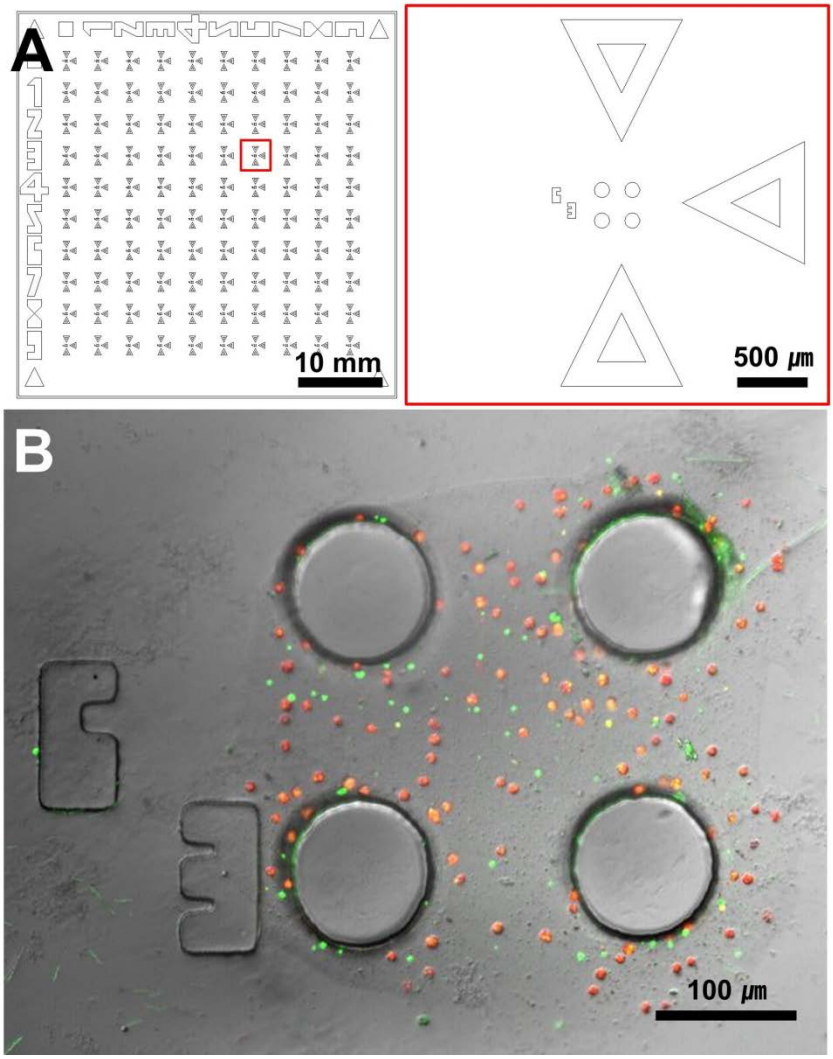

Figure 3. 15　Design of sample collecting device and patterned cell on that device.　(A) CAD design of sample collecting device.　(B) Patterned C. reinhardtii mixed with alginate gel on the sample collecting device.

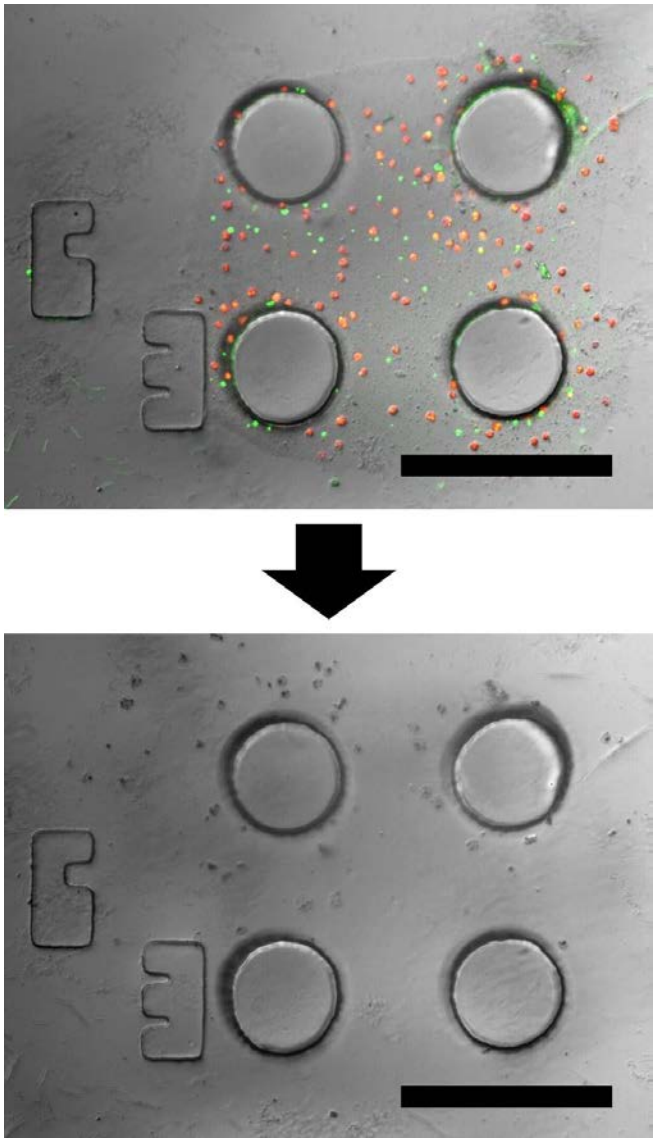

Figure 3. 16 Result of sample collecting. Scale ber = 200 μm

3.3.6 Automatic system for continuous patterning

Strictly speaking, the wiping method which is described in this thesis is not a real high-throughput screening because it needs wiping motions by hands. To overcome this inconvenience, we developed the automatic liquid patterning system for continuous liquid patterning. Figure 3.17 the automatic liquid pattering system. The automatic system consist of DC (direct current) supply system, DC motor and gear box, rubber roller, railway and wiper. The rubber roller transport microstructure-embossed PS(polystyrene) film through the PDMS wiper. Transporting speed can be modulated between 1 to 20 mm/s. During the transporting, PS film passes through the PDMS wiper and microliquid patterns are spontaneously generated. This system provides stable wiping speed and uniform wiping contact area, so the quality of microliquid patterns is better than microliquids patterns generated by hands. (Figure 3.18)

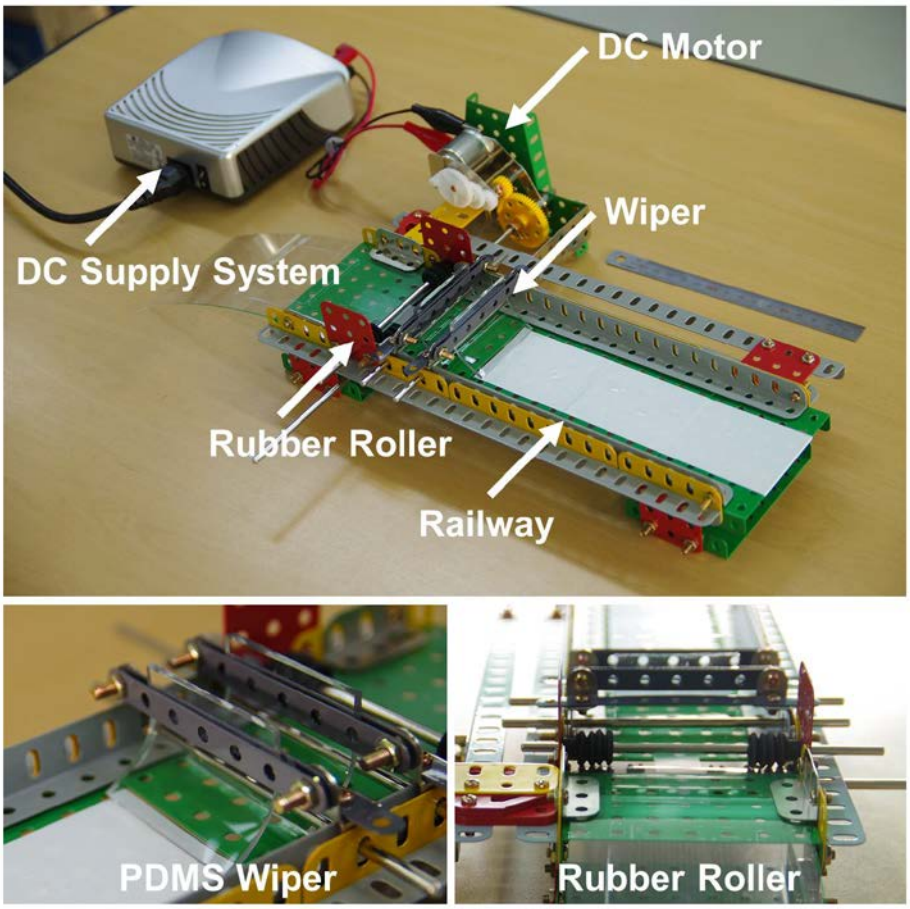

Figure 3. 17 Automatic liquid patterning system

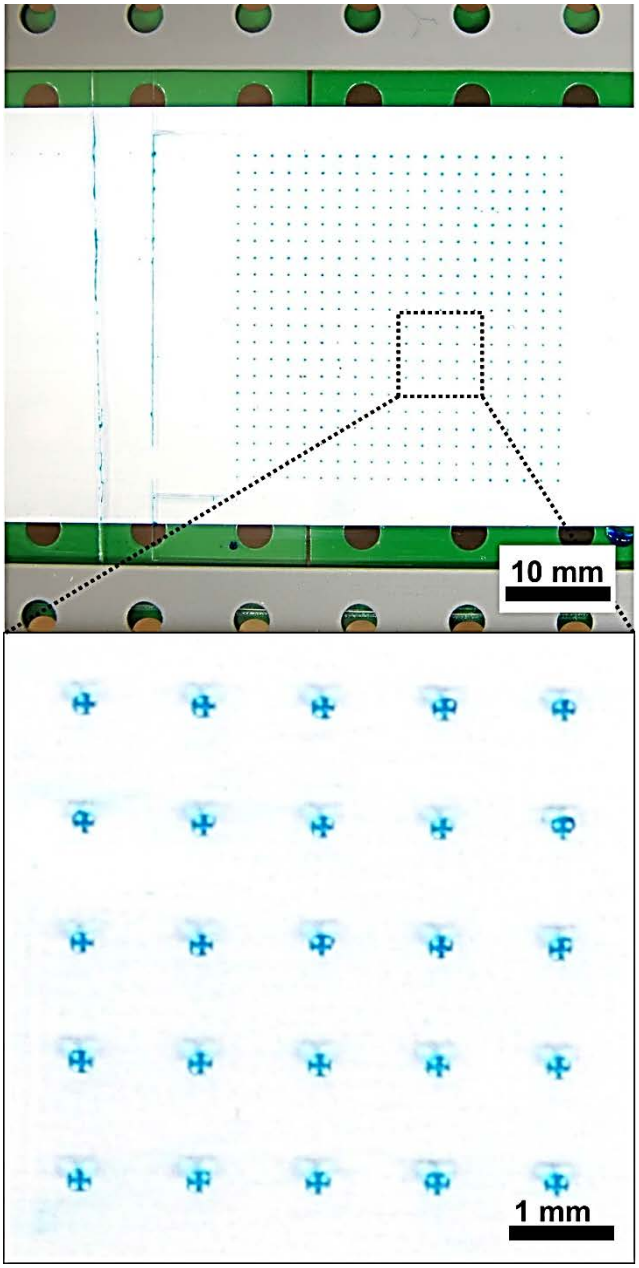

Figure 3. 18 Microliquid array patterned by automatic liquid patterning system

3.4 Conclusion

In this chapter, we developed a liquid patterning method by simple wiping motion based on the meniscus dynamics when liquid moves on the microstructures embossed surfaces. When liquid pass through the microstructures, liquid trapping takes place as advancing menisci snap, merge and generate isolated microliquids inside strategically arrayed microstructures. This liquid motion shows similar patterns as the capillarity guided patterning inside microchannel mentioned in previous chapter. The capillarity guided patterning process on large surface is also robust, reproducible under variable experimental conditions. Nanoliter scale liquids or gels containing cells can be patterned over large areas. The patterning process is extremely simple, fast and can be applied to large surface. One noticeable feature of wiping method is that the surface property is not a major variable. Liquid patterns are generated on both

hydrophilic and hydrophobic surfaces by wiping method.

Another noticeable application of capillarity guided patterning on large surface is sample collecting. We designed novel but simple microstructure arrays contain coordinates and indicators which provide exact position of each liquid patterns. Using this patterned substrate, we can find interesting samples by naked eyes and can collect samples with typical pipettes because the top of patterns is opened.

Moreover, to realize the real high-throughput screening, we designed and demonstrated automatic liquid patterning system which can pattern microliquids automatically.

We believe that the simplicity and robustness of the wiping method will be attractive for a number of biological experimental platforms such as high-throughput screening and Organ-on-a-chip.

Chapter 4.

Concluding Remarks

In this thesis, we suggested new simple liquid patterning methods called capillarity guided patterning of microliquids to produce a lot of liquid patterns including cells inside or outside microchannels. This methods use the meniscus dynamics via microstructures and liquid.

In chapter 2, a new liquid patterning method using surface tension called ‘Capillarity guided patterning (CGP)’ was introduced. Liquid patterning by CGP was performed using strategically placed microstructures inside microchannel. Liquid patterning process was done by simple two steps; fill the microchannel with liquid and drain the microchannel. Then microliquids were spontaneously trapped

inside microstructure arrays. We analyzed the principle of CGP based on hydrodynamic insights and verified by computer simulation and experiments. Using CGP, we demonstrated various liquid patterns including multiple cells for on chip drug screening and organ-on-a-chip applications.

In chapter 3, another liquid patterning method based on CGP was introduced. This method was modified CGP for applying to open surface (not inside channel). This new method also used embossed microstructures but liquid patterning was done by simple wiping motion. This method could be applied to larger area and could be applied to both hydrophilic and hydrophobic surfaces. We demonstrated variety of liquid patterns with cells. Also, the liquid patterns generated by this method can be collected because the liquid patterns are opened to air.

Here we described new microliquid patterning method, named capillarity guided patterning. The most advantageous feature of CGP is simplicity. We believe CGP can be a new paradigm of liquid patterning for large scale drug screening or other lab-on-a-chip research fields.

Bibliography

1. Xia, Y.; Whitesides, G. M., *Annual review of materials science* **1998,** *28* (1), 153-184.

2. Duffy, D. C.; McDonald, J. C.; Schueller, O. J.; Whitesides, G. M., *Analytical chemistry* **1998,** *70* (23), 4974-4984.

3. Carr, J. A.; Parashar, A.; Gibson, R.; Robertson, A. P.; Martin, R. J.; Pandey, S., *Lab on a chip* **2011,** *11* (14), 2385-2396.

4. Dittrich, P. S.; Manz, A., *Nature Reviews Drug Discovery* **2006,** *5* (3), 210-218.

5. Jiang, Y.; Wang, P.-C.; Locascio, L. E.; Lee, C. S., *Analytical chemistry* **2001,** *73* (9), 2048-2053.

6. Whitesides, G. M.; Ostuni, E.; Takayama, S.; Jiang, X.; Ingber, D. E., *Annual review of biomedical engineering* **2001,** *3*, 335-73. DOI 10.1146/annurev.bioeng.3.1.335.

7. Taylor, A. M.; Blurton-Jones, M.; Rhee, S. W.; Cribbs, D. H.; Cotman, C. W.; Jeon, N. L., *Nature Methods* **2005,** *2* (8), 599-605.

8. Di Carlo, D.; Aghdam, N.; Lee, L. P., *Analytical chemistry* **2006,** *78* (14), 4925-4930.

9. Di Carlo, D.; Wu, L. Y.; Lee, L. P., *Lab on a Chip* **2006,** *6* (11), 1445-1449.

10. Lindström, S.; Andersson-Svahn, H., *Lab on a Chip* **2010,** *10* (24), 3363-3372.

11. Osada, K.; Hosokawa, M.; Yoshino, T.; Tanaka, T., *Analyst* **2014,** *139* (2), 425-430. DOI 10.1039/C3AN01698F.

12. Andersson, H.; van den Berg, A., *Sensors and Actuators B: Chemical* **2003,** *92* (3), 315-325. DOI 10.1016/s0925-4005(03)00266-1.

13. Rhee, S. W.; Taylor, A. M.; Tu, C. H.; Cribbs, D. H.; Cotman,

C. W.; Jeon, N. L., *Lab Chip* **2005,** *5* (1), 102-107.
14. Hahn, M. S.; Miller, J. S.; West, J. L., *Advanced Materials* **2006,** *18* (20), 2679-2684.
15. Lee, H.; Kim, S.; Chung, M.; Kim, J. H.; Jeon, N. L., *Microvascular research* **2014,** *91*, 90-98.
16. Lee, H.; Chung, M.; Jeon, N. L., *MRS bulletin* **2014,** *39* (01), 51-59.
17. Hasan, A.; Memic, A.; Annabi, N.; Hossain, M.; Paul, A.; Dokmeci, M. R.; Dehghani, F.; Khademhosseini, A., *Acta biomaterialia* **2014,** *10* (1), 11-25.
18. Hong, J.; Edel, J. B.; deMello, A. J., *Drug Discovery Today* **2009,** *14* (3), 134-146.
19. Wlodkowic, D.; Faley, S.; Zagnoni, M.; Wikswo, J. P.; Cooper, J. M., *Analytical chemistry* **2009,** *81* (13), 5517-5523.
20. Huh, D.; Matthews, B. D.; Mammoto, A.; Montoya-Zavala, M.; Hsin, H. Y.; Ingber, D. E., *Science* **2010,** *328* (5986), 1662-1668.
21. Huh, D.; Torisawa, Y.-s.; Hamilton, G. A.; Kim, H. J.; Ingber, D. E., *Lab on a Chip* **2012,** *12* (12), 2156-2164.
22. Wilbur, J. L.; Kumar, A.; Biebuyck, H. A.; Kim, E.; Whitesides, G. M., *Nanotechnology* **1996,** *7* (4), 452.
23. Qin, D.; Xia, Y.; Whitesides, G. M., *Nature protocols* **2010,** *5* (3), 491-502. DOI 10.1038/nprot.2009.234.
24. Bodas, D.; Khan-Malek, C., *Sensors and Actuators B: Chemical* **2007,** *123* (1), 368-373.
25. Truskett, V. N.; Watts, M. P., *TRENDS in Biotechnology* **2006,** *24* (7), 312-317.
26. Huang, C. P.; Lu, J.; Seon, H.; Lee, A. P.; Flanagan, L. A.; Kim, H.-Y.; Putnam, A. J.; Jeon, N. L., *Lab on a Chip* **2009,** *9* (12), 1740-1748.
27. Shin, Y.; Han, S.; Jeon, J. S.; Yamamoto, K.; Zervantonakis, I.

K.; Sudo, R.; Kamm, R. D.; Chung, S., *Nature protocols* **2012,** *7* (7), 1247-1259.

28. Chung, S. E.; Park, W.; Shin, S.; Lee, S. A.; Kwon, S., *Nature materials* **2008,** *7* (7), 581-587.

29. Hahn, M. S.; Taite, L. J.; Moon, J. J.; Rowland, M. C.; Ruffino, K. A.; West, J. L., *Biomaterials* **2006,** *27* (12), 2519-2524.

30. El Debs, B.; Utharala, R.; Balyasnikova, I. V.; Griffiths, A. D.; Merten, C. A., *Proceedings of the National Academy of Sciences* **2012,** *109* (29), 11570-11575.

31. Zheng, X. T.; Yu, L.; Li, P.; Dong, H.; Wang, Y.; Liu, Y.; Li, C. M., *Advanced drug delivery reviews* **2013**.

32. Gu, W.; Zhu, X.; Futai, N.; Cho, B. S.; Takayama, S., *Proceedings of the National Academy of Sciences of the United States of America* **2004,** *101* (45), 15861-15866.

33. Tung, Y.-C.; Torisawa, Y.-s.; Futai, N.; Takayama, S., *Lab on a Chip* **2007,** *7* (11), 1497-1503. DOI 10.1039/B708187A.

34. Gossett, D. R.; Weaver, W. M.; Ahmed, N. S.; Di Carlo, D., *Annals of biomedical engineering* **2011,** *39* (4), 1328-1334.

35. Park, M. C.; Hur, J. Y.; Kwon, K. W.; Park, S.-H.; Suh, K. Y., *Lab on a Chip* **2006,** *6* (8), 988-994. DOI 10.1039/B602961B.

36. Casavant, B. P.; Berthier, E.; Theberge, A. B.; Berthier, J.; Montanez-Sauri, S. I.; Bischel, L. L.; Brakke, K.; Hedman, C. J.; Bushman, W.; Keller, N. P., *Proceedings of the National Academy of Sciences* **2013,** *110* (25), 10111-10116.

37. Huang, X.; Hui, W.; Hao, C.; Yue, W.; Yang, M.; Cui, Y.; Wang, Z., *Small* **2014,** *10* (4), 758-765.

38. Qin, D.; Xia, Y.; Whitesides, G. M., *Nature protocols* **2010,** *5* (3), 491-502.

39. Kang, L.; Hancock, M. J.; Brigham, M. D.; Khademhosseini, A., *Journal of biomedical materials research Part A* **2010,** *93* (2),

547-557.
40. Huh, D.; Hamilton, G. A.; Ingber, D. E., *Trends in cell biology* **2011,** *21* (12), 745-754.
41. Gerlach, A.; Knebel, G.; Guber, A.; Heckele, M.; Herrmann, D.; Muslija, A.; Sshaller, T., *Microsystem Technologies* **2002,** *7* (5-6), 265-268.
42. Hung, P. J.; Lee, P. J.; Sabounchi, P.; Aghdam, N.; Lin, R.; Lee, L. P., *Lab on a Chip* **2005,** *5* (1), 44-48.
43. Yin, H.; Marshall, D., *Current opinion in biotechnology* **2012,** *23* (1), 110-119.
44. Valencia, P. M.; Farokhzad, O. C.; Karnik, R.; Langer, R., *Nature nanotechnology* **2012,** *7* (10), 623-629.
45. Beebe, D. J.; Mensing, G. A.; Walker, G. M., *Annual review of biomedical engineering* **2002,** *4*, 261-86. DOI 10.1146/annurev.bioeng.4.112601.125916.
46. Dunnett, S. B.; Björklund, A., *Brain Research Protocols* **1997,** *1* (1), 91-99.
47. Abbas, Y.; Miwa, J.; Zengerle, R.; von Stetten, F., *Micromachines* **2013,** *4* (1), 80-89.
48. Ionescu-Zanetti, C.; Shaw, R. M.; Seo, J.; Jan, Y.-N.; Jan, L. Y.; Lee, L. P., *Proceedings of the National Academy of Sciences of the United States of America* **2005,** *102* (26), 9112-9117.
49. Park, J. Y.; Hwang, C. M.; Lee, S.-H., *Biomedical microdevices* **2009,** *11* (1), 129-133.
50. Lee, Y.; Kim, J.; Chung, S.; Chung, C.; Chang, J.; Yoo, J. In *Flow characteristics of hydrophilic/hydrophobic capillaries considering surface tension*, Microtechnologies in Medicine & Biology 2nd Annual International IEEE-EMB Special Topic Conference on, IEEE: **2002**; pp 560-564.
51. Suk, J. W.; Cho, J.-H., *Journal of micromechanics and*

microengineering **2007,** *17* (4), N11.
52. Kudryashov, V.; Yuan, X. C.; Cheong, W. C.; Radhakrishnan, K., *Microelectronic engineering* **2003,** *67*, 306-311.
53. Neuži, P.; Giselbrecht, S.; Länge, K.; Huang, T. J.; Manz, A., *Nature reviews Drug discovery* **2012,** *11* (8), 620-632.
54. Wlodkowic, D.; Cooper, J. M., *Current opinion in chemical biology* **2010,** *14* (5), 556-567.
55. Fernandes, T. G.; Diogo, M. M.; Clark, D. S.; Dordick, J. S.; Cabral, J. M., *Trends in biotechnology* **2009,** *27* (6), 342-349.
56. Crane, M. M.; Chung, K.; Stirman, J.; Lu, H., *Lab on a Chip* **2010,** *10* (12), 1509-1517.
57. Kimura, H.; Yamamoto, T.; Sakai, H.; Sakai, Y.; Fujii, T., *Lab on a Chip* **2008,** *8* (5), 741-746.
58. Tan, W.-H.; Takeuchi, S., *Proceedings of the National Academy of Sciences* **2007,** *104* (4), 1146-1151.
59. Liu, V. A.; Bhatia, S. N., *Biomedical Microdevices* **2002,** *4* (4), 257-266.
60. Khademhosseini, A.; Yeh, J.; Eng, G.; Karp, J.; Kaji, H.; Borenstein, J.; Farokhzad, O. C.; Langer, R., *Lab on a Chip* **2005,** *5* (12), 1380-1386.
61. Wang, Z.; Kim, M.-C.; Marquez, M.; Thorsen, T., *Lab on a Chip* **2007,** *7* (6), 740-745.
62. Smout, M. J.; Kotze, A. C.; McCarthy, J. S.; Loukas, A., *PLoS neglected tropical diseases* **2010,** *4* (11), e885.
63. Revzin, A.; Russell, R. J.; Yadavalli, V. K.; Koh, W.-G.; Deister, C.; Hile, D. D.; Mellott, M. B.; Pishko, M. V., *Langmuir* **2001,** *17* (18), 5440-5447.
64. Leu, T.-S.; Chang, P.-Y., *Sensors and Actuators A: Physical* **2004,** *115* (2), 508-515.
65. Novik, E.; Maguire, T. J.; Chao, P.; Cheng, K.; Yarmush, M.

L., *Biochemical pharmacology* **2010,** *79* (7), 1036-1044.
66. Miller, O. J.; El Harrak, A.; Mangeat, T.; Baret, J.-C.; Frenz, L.; El Debs, B.; Mayot, E.; Samuels, M. L.; Rooney, E. K.; Dieu, P., *Proceedings of the National Academy of Sciences* **2012,** *109* (2), 378-383.
67. Boedicker, J. Q.; Li, L.; Kline, T. R.; Ismagilov, R. F., *Lab on a Chip* **2008,** *8* (8), 1265-1272.
68. Wolfe, D. B.; Qin, D.; Whitesides, G. M., *Methods Mol Biol* **2010,** *583*, 81-107. DOI 10.1007/978-1-60327-106-6_3.
69. Kim, J.; Taylor, D.; Agrawal, N.; Wang, H.; Kim, H.; Han, A.; Rege, K.; Jayaraman, A., *Lab on a chip* **2012,** *12* (10), 1813-1822.
70. Wu, M.-H.; Huang, S.-B.; Lee, G.-B., *Lab on a Chip* **2010,** *10* (8), 939-956.
71. Sia, S. K.; Whitesides, G. M., *Electrophoresis* **2003,** *24* (21), 3563-3576.
72. Dove, A., *Nature biotechnology* **1999,** *17* (9), 859-864.
73. Toh, Y.-C.; Lim, T. C.; Tai, D.; Xiao, G.; van Noort, D.; Yu, H., *Lab on a Chip* **2009,** *9* (14), 2026-2035.
74. Zhao, L.; Cheng, P.; Li, J.; Zhang, Y.; Gu, M.; Liu, J.; Zhang, J.; Zhu, J.-J., *Analytical chemistry* **2009,** *81* (16), 7075-7080.
75. Hung, P. J.; Lee, P. J.; Sabounchi, P.; Lin, R.; Lee, L. P., *Biotechnology and bioengineering* **2005,** *89* (1), 1-8.
76. Huang, H.; Yang, W.; Wang, T.; Chuang, T.; Fu, C., *Journal of Micromechanics and Microengineering* **2007,** *17* (2), 291-296. DOI 10.1088/0960-1317/17/2/015.
77. Clausell-Tormos, J.; Lieber, D.; Baret, J.-C.; El-Harrak, A.; Miller, O. J.; Frenz, L.; Blouwolff, J.; Humphry, K. J.; Köster, S.; Duan, H., *Chemistry & biology* **2008,** *15* (5), 427-437.
78. Xu, F.; Wu, J.; Wang, S.; Durmus, N. G.; Gurkan, U. A.; Demirci, U., *Biofabrication* **2011,** *3* (3), 034101.

79. Ye, N.; Qin, J.; Shi, W.; Liu, X.; Lin, B., *Lab on a Chip* **2007,** *7* (12), 1696-1704.
80. Tokuyama, T.; Fujii, S.-i.; Sato, K.; Abo, M.; Okubo, A., *Analytical chemistry* **2005,** *77* (10), 3309-3314.
81. Rohde, C. B.; Zeng, F.; Gonzalez-Rubio, R.; Angel, M.; Yanik, M. F., *Proceedings of the National Academy of Sciences* **2007,** *104* (35), 13891-13895.
82. Jeon, N. L.; Choi, I. S.; Xu, B.; Whitesides, G. M., *Advanced Materials* **1999,** *11* (11), 946-950.
83. King, E.; Xia, Y.; Zhao, X. M.; Whitesides, G. M., *Advanced Materials* **1997,** *9* (8), 651-654.
84. Deng, T.; Wu, H.; Brittain, S. T.; Whitesides, G. M., *Anal Chem* **2000,** *72* (14), 3176-80.
85. Chen, C.; Hirdes, D.; Folch, A., *Proceedings of the National Academy of Sciences* **2003,** *100* (4), 1499.
86. Wang, Y.; Balowski, J.; Phillips, C.; Phillips, R.; Sims, C. E.; Allbritton, N. L., *Lab on a Chip* **2011,** *11* (18), 3089-3097.
87. Suh, K. Y.; Kim, Y. S.; Lee, H. H., *Advanced Materials* **2001,** *13* (18), 1386.
88. Whitesides, G. M., *Nature* **2006,** *442* (7101), 368-373.
89. Jang, K.; Sato, K.; Igawa, K.; Chung, U.-i.; Kitamori, T., *Analytical and bioanalytical chemistry* **2008,** *390* (3), 825-832.

초 록

미세유체 기반의 실험 플랫폼은 생물학적 및 화학적 현상을 연구하기 위한 기법으로 널리 쓰이고 있다. 특히 소프트 리소그래피를 비롯한 기타 방법들이 기존의 포토 리소그래피 기반의 방법을 대체하기 위해 연구되고 있으며 많은 연구자들에 의해 기존의 페트리 접시 기반의 방법에 비해 월등한 성능을 갖는 새로운 플랫폼들이 개발되고 있으나 그 방법들 역시 비용 및 적용 부분에서 발전 시켜야 할 부분들이 많다. 본 논문에서는 미소 단위의 액체를 빠르고 간단하게 패터닝 할 수 있는 새로운 방법을 소개한다. 본 방법은 유체와 미세 구조물 사이에 작용하는 표면 장력에 의해 형성되는 계면 모양의 변화를 이용하여 액체를 패터닝 하는 방법이다. 유체의 패터닝은 전략적으로 배열된 미세 구조물 상에 유체를 흘려 준 후 유체를 이동 시키면 추가적인 공정이 필요 없이 표면 장력에 의해 원하는 위치에 1 nL 의 유체가 패터닝 된다. 이 방법은 유체역학 및 시뮬레이션에 의해 분석되었고 실험을 통하여 그 방법 및 이론적 해석을 검증하였다. 본 방법에 의해 물을 비롯한 여러 액체를 여러 가지 모양 및 크기로 수 초 이내에 패터닝 하는데 성공하였으며 이를 이용하여 세포를 패터닝 함으로서 새로운 스크리닝 플랫폼으로서의 가능성을 보였다. 본 방법은 유체를 패터닝 하는 새로운 방법으로서 많은 체외 실험 모델에 널리 쓰일 수 있을 것으로 기대된다.

주요어: 랩온어칩, 유체 패터닝, 미세유체, 표면장력, 고효율스크리닝, 장기모사칩

학 번: 2012-30732